

Review

Protection of Multi-Terminal HVDC Grids: A Comprehensive Review

Mohamed Radwan  and Sahar Pirooz Azad * 

Electrical and Computer Engineering, University of Waterloo, 200 University Ave W,
Waterloo, ON N2L 3G1, Canada

* Correspondence: sahar.azad@uwaterloo.ca

Abstract: Multi-terminal HVDC grids facilitate the integration of various renewable resources from distant locations; in addition, they enhance the reliability and stability of the grid. Protection is one of the major obstacles in realizing reliable and secure multi-terminal HVDC grids. This paper presents a comprehensive review of the existing protection schemes for multi-terminal HVDC grids. First, DC fault current stages are demonstrated; in addition, fault analysis studies and the existing fault current calculation methods are reviewed. Then, HVDC grid protection requirements including multi-vendor interoperability conditions are extensively discussed. Furthermore, primary protection algorithms are classified into single- and double-ended schemes, and a detailed comparison between each category is presented such that the distinctive algorithms from each group are highlighted. Moreover, the recent DC reclosing schemes are reviewed highlighting their role in enhancing grid stability and ensuring supply continuity. Finally, available standards for HVDC protection systems alongside their design considerations and procedures are thoroughly outlined. This paper focuses on the recently proposed methods to design reliable protection schemes for multi-terminal HVDC grids and highlights the main advantages and disadvantages associated with them; thus, it offers a beneficial guide for researchers in the HVDC protection field.

Keywords: HVDC grid protection; MMC converters; double-ended schemes; single-ended schemes; protection strategies; DC circuit breakers; DC fault location; reclosing schemes



Citation: Radwan, M.; Azad, S.P. Protection of Multi-Terminal HVDC Grids: A Comprehensive Review. *Energies* **2022**, *15*, 9552. <https://doi.org/10.3390/en15249552>

Academic Editor: Hao Wu

Received: 3 November 2022

Accepted: 14 December 2022

Published: 16 December 2022

Publisher's Note: MDPI stays neutral with regard to jurisdictional claims in published maps and institutional affiliations.



Copyright: © 2022 by the authors. Licensee MDPI, Basel, Switzerland. This article is an open access article distributed under the terms and conditions of the Creative Commons Attribution (CC BY) license (<https://creativecommons.org/licenses/by/4.0/>).

1. Introduction

HVDC corridors play an essential role in integrating renewable energy resources (RESs), harvesting their power, and feeding it into the power grid, especially offshore wind farms, which are interconnected to the onshore grid via submarine HVDC cables [1]. Furthermore, grid stability issues resulting from uncertainty, volatility, and intermittency of wind energy sources become more controllable with HVDC interconnections rather than direct AC interconnections [2]. Moreover, the distance between the offshore wind platform and the onshore interfacing point of connection adds another restriction on utilizing submarine AC cables since their charging currents increase for long distances and the compensation cost for these currents will be high, whereas submarine DC cables have nearly negligible charging currents [3]. An example of such an offshore wind harvesting multi-terminal HVDC grid is the proposed Atlantic wind connection (AWC) project that is intended to collect up to 7 GW of offshore wind power over the eastern coast of the United States [4].

HVDC systems can be classified based on the converter technology into line-commutated converters (LCCs) and voltage-sourced converters (VSCs). VSCs exhibit various operational merits over LCCs as highlighted in Table 1 [5,6]. In addition, the constant DC link voltage of VSCs facilitates their parallel operation, which is an important feature to build multi-terminal HVDC grids. Modular multilevel converters (MMCs) are extensively exploited in recent HVDC projects and will be used in future projects due to

their notable features such as modularity, scalability, low switching frequency and losses, and low filtering requirements [7–10]. Numerous HVDC projects have been installed and commissioned worldwide, ranging from point-to-point connections to multi-terminal HVDC grids. China and Europe possess the dominant share of these projects. For instance, the Chinese power utility is recognized as the largest hybrid DC-AC grid worldwide with more than 50 HVDC projects in service and a capacity greater than 70 GW [11]. Table 2 presents a brief overview of a selected number of the existing large HVDC projects.

Table 1. Comparison between LCCs and VSCs.

Comparison Aspect	LCCs	VSCs
Semiconductor switch	Thyristor	IGBT
Switch controllability	Semi-controllable	Fully-controllable
Commutation failure	Yes	No
DC Link	Constant current polarity	Constant voltage polarity
Power reversal	Slow (requires voltage reversal)	Simple and fast (no need for voltage reversal)
Harmonics	Low-order harmonics	High-order harmonics
Filter Size	Large	Small
Active and Reactive Power Control	Coupled control	Decoupled control
Reactive Compensation Requirement	Yes	No
Reactive support provision	No	Yes
Black-start capability	No	Yes

Table 2. Existing HVDC projects overview.

HVDC Project	Country	Commissioning Year	Capacity	DC Voltage Level	Grid Configuration	Number of Terminals
Zhangbei [12]	China	2021	4.5 GW	±500 kV	Meshed	Four ¹
NordLink [13]	Germany/Norway	2021	1.4 GW	±525 kV	Point-to-point	Two
North Sea Link ² [14]	Norway/UK	2021	1.4 GW	±525 kV	Point-to-point	Two
Wudongde [15]	China	2020	8 GW	±800 kV	Star-connected	Three
Changji-Guquan ³ [16]	China	2019	12 GW	±1100 kV	Point-to-point	Two
Maritime Link [17]	Canada	2018	500 MW	±200 kV	Point-to-point	Two
Zhoushan [18]	China	2014	1 GW	±200 kV	Meshed	Five ⁴
Nan'ao [19]	China	2013	200 MW	±160 kV	Star-connected	Three

¹ This project will be extended to six terminals in the second phase [11]. ² The world's longest submarine interconnector with 720 km length. ³ This is the largest HVDC project worldwide in terms of transmission distance, DC voltage rating, and power transfer capability. ⁴ World's first five-terminal HVDC project.

Protection is one of the major obstacles in realizing reliable and secure multi-terminal HVDC grids. Implementation of a reliable, sensitive, and selective protection system for HVDC networks is more challenging as compared to conventional AC systems, since DC faults result in a large and nearly instantaneous rise of the DC current, which has no zero-crossings. The large DC fault current is due to the low-impedance, low-inertia of HVDC

networks and the rapid discharge rate of the converters' capacitors. This issue imposes stringent constraints on the fault clearing time to be in the range of a few milliseconds, e.g., 6 ms for the Zhangbei HVDC project [20], including 3 ms for the fault interruption process; thus, requiring the design of ultra-fast protection schemes along with fast fault current interrupters such as direct current circuit breakers (DCCBs) that can interrupt the fault current in the absence of a zero-crossing.

Several HVDC protection schemes are proposed in the literature. There are two main classifications for HVDC protection algorithms; first, they can be classified based on the intended protection function and speed into primary and backup protection schemes similar to AC protection systems. Second, protection algorithms can be classified into single-ended (communication-less or non-pilot) and double-ended (communication-based or pilot) schemes based on their need for a communication channel. An example of pilot schemes is the HVDC differential protection scheme, which is inspired by AC differential algorithms, yet DC schemes are more challenging to design due to long transmission lines and the rigid data-synchronization requirements of the communication system.

Single-ended schemes have been proposed mainly to compensate for the delayed operation of double-ended schemes due to communication delays. Therefore, local-measurement-based schemes become essential in order to realize ultra-fast fault detection and classification. The proposed methodologies depend on various criteria such as detecting the sudden change of transient fault currents and voltages [21]. In addition, inspired by AC protection principles, fault induced traveling waves have been broadly utilized in DC systems. Their distinctive features, which carry the fault signature, are extracted by employing well-known mathematical signal processing tools such as Fourier and wavelet transforms [22,23].

This paper presents a comprehensive review of VSC-HVDC grid protection schemes. Other valuable reviews are presented in [24–26]. Compared with these reviews, the major contributions of this paper are summarized as follows: (1) this paper exclusively focuses on the proposed protection algorithms for VSC-based HVDC grids since the majority of the current and planned HVDC projects are based on VSCs; (2) recent schemes are intensively reviewed, highlighting the current research trends and methodologies of HVDC protection schemes; (3) protection algorithms are classified into single- and double-ended schemes and a detailed comparison between each category is presented such that the distinctive algorithms from each group are highlighted; (4) fault analysis studies and the proposed fault current calculation methods are reviewed; (5) HVDC grid protection requirements including multi-vendor interoperability conditions are extensively discussed; (6) recent DC reclosing schemes, which have not been discussed in the existing review papers, are reviewed highlighting their role in enhancing grid stability and ensuring supply continuity; and (7) available standards for HVDC protection systems alongside their design considerations and procedures are thoroughly outlined.

The rest of the paper is organized as follows: in Section 2, DC fault phenomenon including the fault stages, calculation methods, and fault clearing strategies are investigated; in addition, fundamental protection requirements for HVDC schemes are discussed. In Section 3, a comprehensive review of primary and backup protection algorithms is provided and the major differences between single- and double-ended primary schemes are addressed. Section 4 focuses on double-ended schemes and provides a comprehensive review of the existing algorithms. A comparable review of single-ended schemes is presented in Section 5. An overview of fault location identification schemes is demonstrated in Section 6. The concept of auto-reclosing in HVDC grids is presented in Section 7 and later the proposed reclosing schemes are reviewed. Design considerations and procedures of HVDC protection systems are addressed in Section 8 in addition to highlighting the available standards related to HVDC grid protection. The conclusions are outlined in Section 9.

2. Fundamentals of DC Faults

As reported in the joint paper of the European network of transmission system operators for electricity (ENTSO-E) and Europacable [27], DC cable faults are scarce and a few cable-fault incidents were historically reported by transmission system operators (TSOs). Root causes of DC cable (underground and submarine) faults are as follows: (1) cable insulation breakdown due to aging or internal partial discharges; (2) uncoordinated digging works; (3) overheating due to persistent overloading operation; (4) improper cable burial; and (5) anchor and pack ice damages. On the other hand, DC faults are more frequent in the case of overhead transmission lines due to their exposure to unexpected and uncontrolled climate conditions. Furthermore, the majority of these faults are temporary (non-permanent). Consequently, auto-reclosing schemes, similar to those employed in AC transmission networks, are needed to ensure supply continuity; thus, reducing the outage time and improving the transmission system reliability [28]. Table 3 summarizes the most common causes of DC faults in various HVDC transmission facilities.

Table 3. Common roots of DC faults.

Employed Transmission Facility	Common Roots	Fault Type	Fault Nature
Overhead Lines	1. Direct lightning strikes.	Pole-To-Ground	Temporary
	2. Indirect back flashover across insulators.	Pole-To-Ground	Temporary
	3. Sudden contact between conductors or between one conductor and ground due to external objects (such as trees or birds).	Pole-To-Ground or Pole-To-Pole	Temporary
	4. Swinging of conductors due to severe storms.	Pole-To-Pole	Temporary
	5. Broken conductors.	Pole-To-Ground	Permanent
	6. Insulation failure due to aging or pollution.	Pole-To-Ground	Permanent
	7. Tower collapse due to natural disasters.	Pole-To-Pole-To-Ground	Permanent
Underground Cables	1. Insulation failure due to aging, overloading, etc.	Pole-To-Ground	Permanent
	2. Uncoordinated digging works.	Pole-To-Ground	Permanent
	3. Improper cable burial.	Pole-To-Ground	Permanent
Submarine (Undersea) Cables	1. Insulation failure due to aging, overloading, etc.	Pole-To-Ground	Permanent
	2. Anchor and pack ice damages.	Pole-To-Ground	Permanent
	3. Fishing gears.	Pole-To-Ground	Permanent

2.1. DC Fault Stages

DC short-circuit fault currents are extremely large due to the small impedance of DC networks [29,30]. Additionally, the fast discharge rate of the converters' capacitors accelerates the rise of the fault current to high levels in the first few milliseconds after the fault incident [31]. Three main stages can be identified during a short-circuit DC fault [32,33]. The first stage is the capacitor discharge stage at which the DC link capacitors or the submodule capacitors of MMCs rapidly discharge into the fault. The high rate of rise of the fault current during this stage triggers the converters' overcurrent protective measures, resulting in the converter blocking. The second stage is the inductive discharge stage caused by cable inductances and arm reactors of MMCs, since inductive currents cannot be instantaneously interrupted after converters are blocked. The third stage, which is automatically triggered after the inductive currents reach zero, is the AC infeed stage where the converters behave as uncontrolled rectifiers feeding the DC-side fault with large steady-state currents from the AC network. It is worth mentioning that DC fault

currents should be interrupted during the first stage to prevent losing the controllability of converters and avoid exceeding the interrupting capabilities of the employed DCCBs [26].

To demonstrate the aforementioned fault current stages, a symmetrical-monopolar half-bridge MMC-based four-terminal HVDC grid, shown in Figure 1, is simulated in PSCAD/EMTDC. The test system, proposed in [34], consists of two offshore wind farms that are interconnected with two AC grids via a four-terminal meshed transmission network consisting of five DC cables. The AC grids have a rated voltage of 400 kV, while the rated voltage of the DC grid is ± 320 kV, which is controlled by the converters at terminals 3 and 4. Active power is controlled by the converters at terminals 1 and 2, while reactive power is controlled by all the converters. The remaining grid parameters are provided in [34]. A pole-to-pole fault at the middle of cable 13 is initiated at 0.71 s. The positive-pole current measured by relay R_{13} is shown in Figure 2. As depicted in Figure 2, the capacitor discharge stage starts at t_{dis} once the first fault-induced backward traveling wave reaches bus 1 and is detected by R_{13} . Then, after a few milliseconds, depending on the initial energy stored in the submodule capacitors, withstanding capabilities of semiconductor switches, and fault parameters, the inductive discharge stage starts at t_{ind} . Finally, the AC infeed stage commences at t_{ac} once the arm inductors are completely discharged.

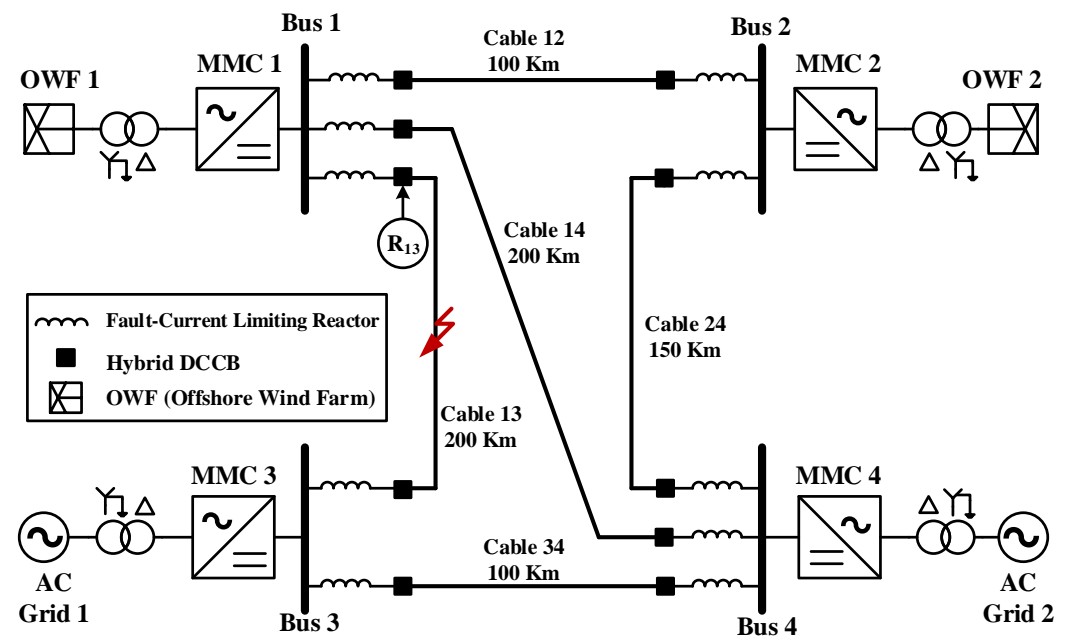


Figure 1. Four-terminal HVDC test grid.

DC fault transients depend on the fault type and the grid's grounding configuration. For instance, pole-to-pole faults always result in significant fault currents and low voltage conditions regardless of the grounding type [35]. On the other hand, system grounding has a significant effect on fault behavior in case of pole-to-ground faults [36]. Variations in fault currents and voltages primarily depend on the grounding type, whether low- or high-impedance grounding is used, as well as the number of grounding points through the HVDC grid [37]. For instance, in the case of low-impedance grounding, pole-to-ground faults cause large short-circuit currents and low voltage conditions similar to pole-to-pole faults [37]. On the contrary, in the case of high-impedance grounding, DC faults result in limited fault currents and large overvoltages on the healthy pole; thus, necessitating additional insulation requirements. Therefore, it can be concluded that the grounding configuration of HVDC grids not only affects the fault behavior but also has a substantial impact on the selection of parameters and ratings of various grid equipment such as the DCCBs.

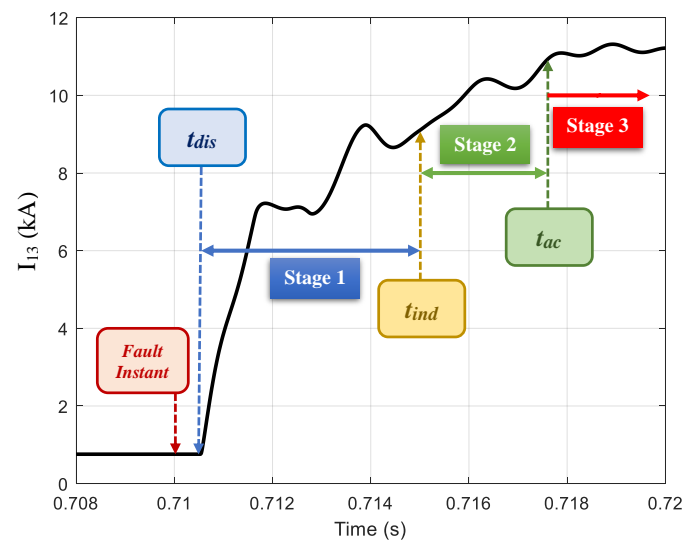


Figure 2. Positive-pole current during various stages of a DC fault.

Limiting the large currents and their high rate of rise during DC fault incidents is crucial to restrict the impact of the resulting stresses on various grid components and guarantee fault current interruption without exceeding switchgear ratings. The grounding impedance is a potential solution to limit fault currents; however, there is a constraint on its value to avoid undesirable overvoltages. Another practical solution is installing DC reactors at both ends of each transmission line or cable segment within the HVDC grid. Fault-limiting or smoothing reactors installed at the converter terminals can effectively limit the fast rise of fault currents; therefore, they prolong the permissible fault clearing time [38]. Furthermore, installing DC reactors enables dividing the HVDC grid into separate protection zones to facilitate the identification of the faulted segment and thus ensuring selectivity. This approach has been widely used in the literature to design HVDC grid protection schemes, particularly single-ended schemes where communication channels are not required [39].

The size of these reactors should be carefully selected since by increasing the reactor size, dynamic stability issues arise with power flow reversal; thus, affecting the control of converters. In addition, large reactors are more expensive and have larger footprints and losses. The minimum reactor size that prevents the blocking of converters during DC fault events can be estimated from the given formula in [38]:

$$L_{dc}^{min} = \frac{1}{2} \frac{u_{dc}}{\Delta I} t_c - \frac{1}{3} L_{arm}, \quad (1)$$

where L_{dc}^{min} is the minimum boundary inductance per pole, L_{arm} is the MMC arm inductance, and ΔI is the permissible current rise within the specified fault clearing time t_c .

2.2. DC Fault Current Calculation

Fault calculations are significantly important to understand the fault phenomenon; hence, selecting a proper fault detection and discrimination criterion such that reliable and selective protection algorithms can be designed. Calculation of voltages and currents associated with DC faults should be accurately performed to determine the ratings of various grid components and precisely adjust the protective relay settings. Precise equivalent models for HVDC grid converters have to be established to obtain an accurate assessment of fault currents. A reduced RLC equivalent circuit model of half-bridge MMCs is proposed in [40], which precisely describes the initial fault stage, i.e., capacitive discharge stage. Therefore, it can be easily used to evaluate various protection algorithms, which are capable of detecting DC faults in this stage, without increasing neither the computational burden nor the simulation time compared to the case when detailed models are employed.

This equivalent model, shown in Figure 3, has been extensively adopted due to its simplicity. The parameters of the equivalent circuit can be calculated from (2)–(4) [41,42]:

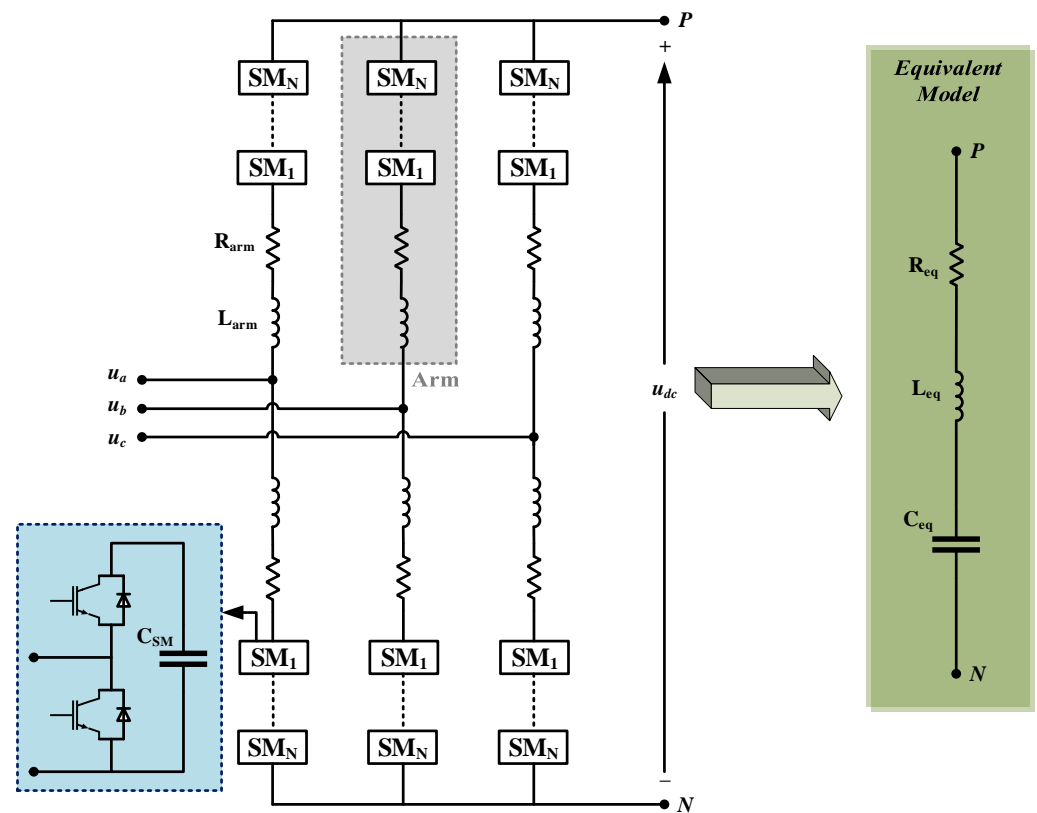


Figure 3. RLC equivalent circuit of a half-bridge MMC [40].

$$R_{eq} = \frac{2}{3}(R_{arm} + N_{SM} R_{on}), \quad (2)$$

$$L_{eq} = \frac{2}{3}L_{arm}, \quad (3)$$

$$C_{eq} = \frac{6 C_{SM}}{N_{SM}}, \quad (4)$$

where R_{eq} , L_{eq} , and C_{eq} are the MMC equivalent resistance, inductance, and capacitance, respectively. R_{arm} is the arm resistance. N_{SM} is the number of submodules per arm. R_{on} is the on-state resistance per submodule, namely, the on-resistance of each IGBT. In the case of full-bridge MMCs, the same equivalent circuit can be adopted considering an on-state resistance twice that of a half-bridge MMC, since two IGBT switches will be turned on per submodule in this case [10]. However, by utilizing this model for full-bridge MMCs, the accuracy of fault current calculations is reduced compared to half-bridge MMCs since the impacts of the converter's control response to the fault, which are inherently ignored by this model, become significant in the case of full-bridge MMCs [43].

Several research studies in the literature have proposed various methods to calculate fault currents with acceptable precision and minimum calculation burden. The recently developed calculation approaches focus on analyzing large multi-terminal MMC-HVDC grids [44–47]. The proposed calculation method in [44] depends on developing the frequency-domain equivalent circuit of the grid during the fault; then, superposition principle is utilized to calculate the fault current. The approach introduced in [45] relies on calculating the prefault and during-fault frequency-domain bus impedance matrices of the grid, then applying inverse Laplace transform to obtain the time-domain fault currents and voltages. In [46], the proposed calculation method is based on modeling the grid with an

equivalent RLC circuit using the companion circuit method. This method greatly reduces the computational burden by converting the network dynamic differential equations into simplified algebraic equations. The resultant circuit is solved by using its equivalent conductance matrix. The approach introduced in [47] simplifies the grid equivalent circuit by modeling the distant converter stations with constant current sources to reduce the grid complexity. In addition, this method has the advantage of considering the mutual coupling between positive and negative poles in the case of asymmetric bipolar grids.

Reference [48] introduces a comprehensive theoretical analysis of fault initiating traveling waves in bipolar MMC-HVDC grids; in addition, detailed expressions describing the grid dynamics are provided. Reference [49] proposes an analytical expression to estimate the contribution of the grid capacitive components to the pole-to-ground fault currents during the first stage of the fault. Moreover, Ref. [50] estimates the individual pole-to-ground fault current contributions from various network components in addition to investigating the parameters impacting these contributions.

2.3. DC Fault Clearing Philosophies

Designing a complete protection system for a multi-terminal HVDC grid requires specifying the strategy used to clear DC faults. A fault clearing strategy (or philosophy) can be defined as the approach taken by the protection system to clear DC faults [51]. According to [52], fault clearing strategies can be classified into three main categories, namely, non-selective, partially-selective, and fully-selective. Based on the desired protection system requirements and the imposed grid constraints, an appropriate protection philosophy is selected [52]. Accordingly, the necessary fault current interrupters are selected and the grid protection zones are specified.

In non-selective fault clearing strategies, the entire HVDC grid is de-energized in the case of DC fault events utilizing either AC circuit breakers (ACCBs) or fault-blocking converters. Then, high-speed switches (HSSs) [53] installed at the ends of each line isolate the faulted segment; therefore, permitting restoration of the remaining healthy portion of the grid. In this strategy, the entire DC grid is considered as one protection zone, as shown in Figure 4. Although there is no selectivity in this strategy, it has a reduced cost since the installation of DCCBs, at line ends, is not required. However, this strategy is more suitable for point-to-point configurations since the loss of the entire HVDC grid during faults will impose severe stability issues.

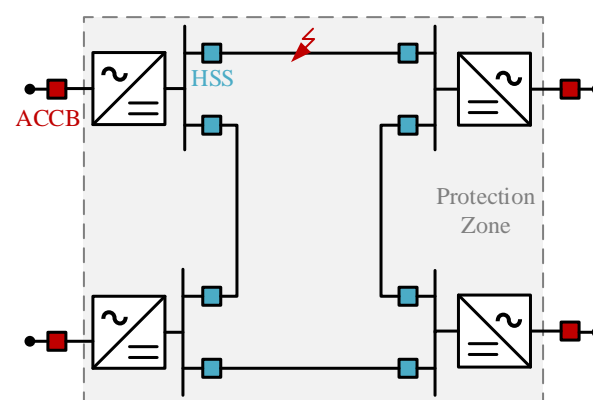


Figure 4. Protection zone of a non-selective fault clearing strategy.

On the contrary, in fully-selective fault clearing strategies, only the faulted segment is tripped without affecting the remaining healthy grid via installing DCCBs at both ends of each segment. This strategy is the most reliable and selective choice for multi-terminal grids since individual protection zones are specified for protecting the various grid components, similar to AC protection systems, as shown in Figure 5. However, the high cost of the required DCCBs is the main disadvantage of this strategy.

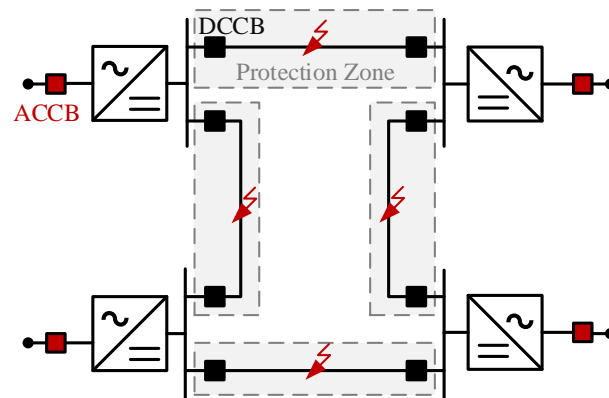


Figure 5. Line protection zones with a fully-selective fault clearing strategy.

A compromised solution is the partially-selective fault clearing strategy or the grid-splitting strategy, where the entire grid is divided into two or more protection zones, called subgrids, separated by interface DCCBs or DC/DC converters, as shown in Figure 6. A fault within a subgrid results in its tripping via the interfacing equipment and ACCBs of the faulted subgrid. Then, HSSs open to isolate the faulted segment, similar to the non-selective philosophy, resulting in the rapid restoration of the healthy part of the isolated subgrid.

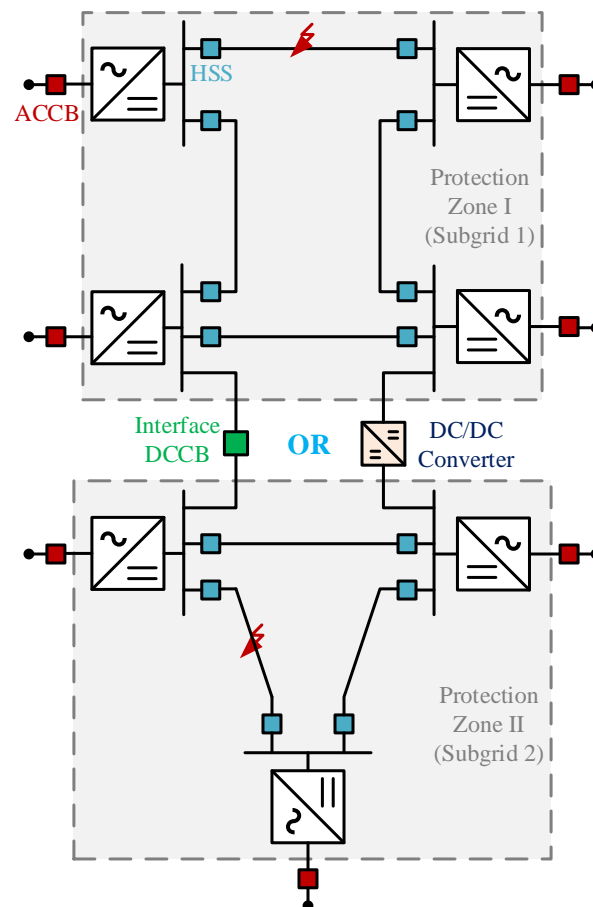


Figure 6. Protection zones with a partially-selective fault clearing strategy.

DCCBs are the major components of fully-selective fault clearing strategies. DCCBs comprise three parallel paths with coordinated conduction during fault events, namely, the main conduction or load current path, the commutation or current-zero creation path, and the energy absorption path [54], as shown in Figure 7. The main conduction path

carries the normal load current, while the role of the commutation path is to transfer the large fault current from the main conduction path into the energy absorption path. The latter path primarily consists of surge arresters, such as metal-oxide varistors (MOVs), that dissipate the fault energy, drive the fault current into zero, and protect DCCB components against transient overvoltages [55]. There are three main types of DCCBs, i.e., mechanical (Figure 8), solid-state (Figure 9), and hybrid (Figure 10). Typical mechanical DCCBs can interrupt fault currents up to 16 kA within 10 ms [56], which is relatively slow. On the other hand, solid-state DCCBs, where normal load current conduction and fault current commutation are achieved by the same branch consisting of a series set of semiconductor switches, can achieve an ultra-fast operation in the range of microseconds due to the absence of mechanical moving parts. Nevertheless, the employed semiconductor switches result in large on-state conduction losses. Hybrid DCCBs are the ultimate topologies that combine the fast operation of solid-state breakers with the reduced conduction losses of mechanical DCCBs. The main conduction path comprises an ultra-fast disconnecter (UFD), which provides instantaneous off-line isolation, and a load commutation switch (LCS), which consists of a reduced set of series semiconductor switches with much lower on-state conduction losses compared to solid-state breakers [57]. For example, in the Zhoushan five-terminal HVDC project, the world's first hybrid DCCBs are installed in 2016 with an interruption capability of 15 kA and an operating time of 3 ms [58]. Moreover, in the Zhangbei four-terminal HVDC project in China, 535 kV hybrid DCCBs are employed that can interrupt fault currents up to 25 kA in less than 3 ms [59]. Mechanical DCCBs are employed in the Nan'ao three-terminal HVDC project in China, commissioned in 2013, which are capable of interrupting fault currents in the range of 9 kA within 5 ms [59].



Figure 7. Generic DCCB layout.

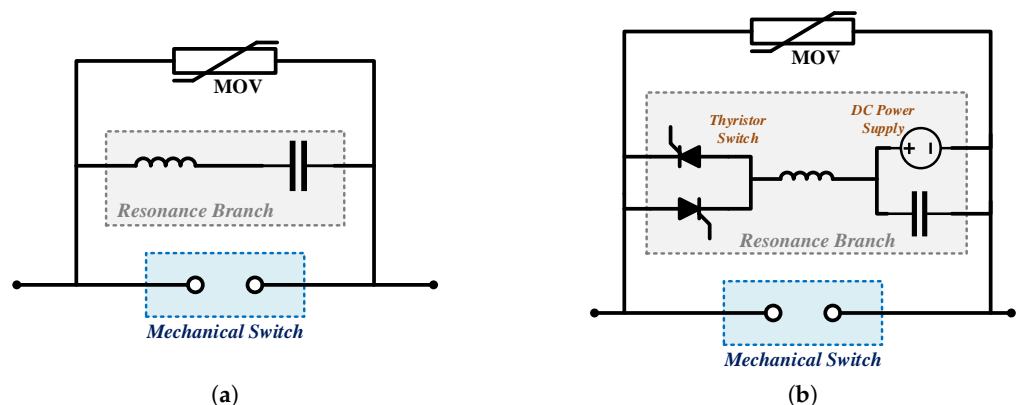


Figure 8. Typical mechanical DCCB topologies: (a) Passive-resonance [55]. (b) Active-resonance [56].

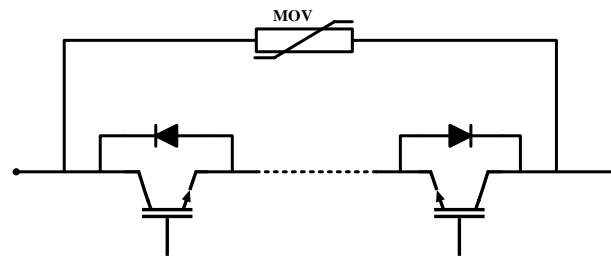


Figure 9. IGBT-based solid-state DCCB [31].

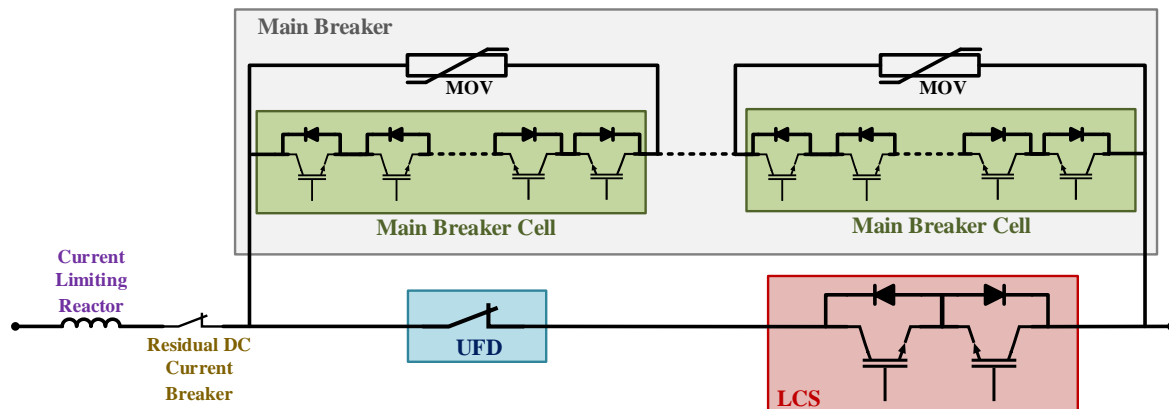


Figure 10. A hybrid DCCB [55].

2.4. HVDC Protection System Requirements

As HVDC systems expand from point-to-point interconnections to multi-terminal grids, protection requirements become more stringent and challenging to be fulfilled. The fundamental protection principles that must be satisfied for multi-terminal HVDC protection schemes are [25,60,61]:

- **Reliability:** similar to the reliability requirements of AC systems, a reliable DC protection system should be dependable, i.e., operate correctly when required in case of all intended faults, and secure, i.e., do not operate incorrectly in case of unintended faults or normal operating conditions.
- **Sensitivity:** the protection algorithm should be sensitive to all internal fault events even those with severe fault conditions such as solid close faults, remote faults, and high-resistance faults.
- **Selectivity:** defined as the ability of the protection scheme to accurately identify the faulted segment and distinguish between internal and external faults.
- **Discrimination:** the protection algorithm should be able to correctly distinguish between forward and reverse faults, identify the fault type (pole-to-pole or pole-to-ground), and determine the faulty pole in case of pole-to-ground faults.
- **Speed:** the protection scheme should initiate a trip signal, in case of internal faults, within a few milliseconds in order to prevent damages to converters' semiconductor switches with limited overcurrent capabilities. Furthermore, fast fault tripping is mandatory to ensure fault clearing before converters are blocked due to overcurrent or undervoltage conditions; thus, avoiding any current contribution from the AC-side towards the fault.
- **Seamlessness:** defined as the ability of the protection scheme to facilitate the stable and secure operation of the remaining healthy portion of the grid after clearing the faulted segment in the case of permanent faults. This requirement will be guaranteed if the aforementioned requirements are properly satisfied.
- **Restoration:** defined as the ability of the employed control and protection system to quickly restore the pre-fault stable operation of the system in case of temporary faults

through either exploiting the fault-tolerant capabilities of fault-blocking converters or utilizing appropriate reclosing strategies.

- **Robustness:** defined as the capability of the protection scheme to detect all fault events in addition to distinguish them from other severe conditions under different operating modes.
- **Computational Burden:** the proposed protection algorithm should detect the faults with low computation requirements and a low sampling frequency in order to comply with high speed requirements.
- **Safety:** the utilized protection system should provide a safe protective shield not only for system components but also for personnel, besides ensuring public safety.
- **Interoperability:** defined as the adaptability of the protection scheme to coordinate with other protection philosophies in the case of multi-vendor multi-terminal grids [62]. Multi-vendor protection interoperability is a crucial step to enable expanding the existing two-terminal links into multi-terminal grids built by multiple vendors; thereby increasing the transmission system transfer capability and improving its reliability at a lower cost [63–65]. Figure 11 summarizes these requirements.



Figure 11. Protection requirements for HVDC grids.

3. HVDC Grid Protection Schemes

A large number of DC protection algorithms have been proposed in the literature with various criteria and methodologies in order to achieve fast and selective fault detection. A suitable protection algorithm should be able to meet the aforementioned protection requirements in Section 2.4. In addition, it should be adaptable so that it can be applied to various converter topologies and grid configurations. Figure 12 shows a detailed classification of HVDC grid protection schemes. Protection schemes can be categorized into primary and backup. Moreover, primary schemes can be further classified, based on the need for remote-terminal information, into single- and double-ended schemes. Figure 12 shows the various principles based on which single-ended and double-ended algorithms are formed. This section discusses the fundamental differences between single- and double-end primary protection schemes. In addition, an overview of the proposed backup protection algorithms is presented.

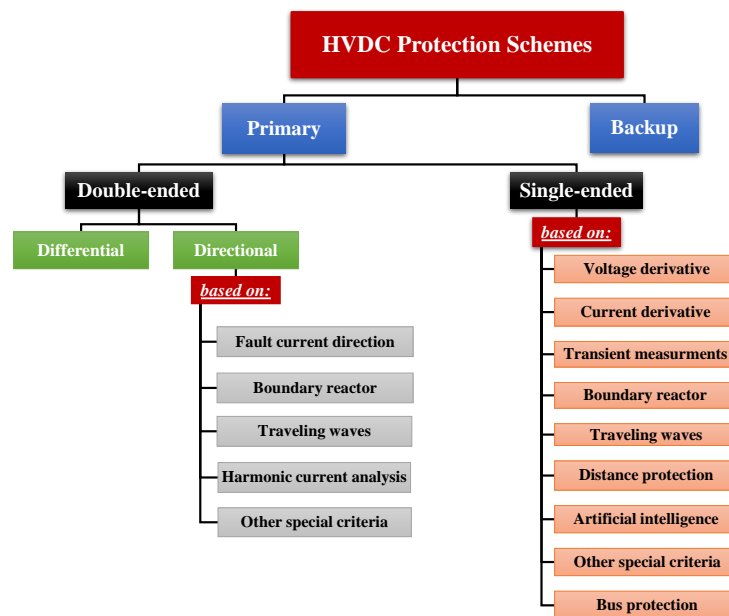


Figure 12. Classification of HVDC grid protection schemes.

3.1. Primary Protection Schemes

HVDC primary protection schemes can be classified into two major categories: double-ended schemes (also called pilot, unit, or communication-based schemes) and single-ended schemes (also called non-pilot, non-unit, or communication-less schemes). The former group utilizes communication channels to exchange measurement data or signals between boundary relays at both ends of each transmission line or cable segment based on which trip or no-trip decisions will be made. On the contrary, for single-ended schemes, only local measurements are required and there is no need for far-end data.

Double-ended schemes are inherently selective, even for severe fault conditions such as high-resistance faults, since protection zones are formed between the boundary relays without the need for DC limiting reactors [66]. However, their slow operation, due to communication delays, is a major shortcoming that impedes their applicability as fast primary protection schemes; yet they can be effectively utilized as backup schemes. Hence, fast communication channels with adequate bandwidth, such as those provided by optical-fiber cables, have to be employed to limit this delay, increase the reliability of these channels, and enhance their immunity against noise such that unit protection schemes can be safely utilized for primary protection [67]. Furthermore, synchronization between the exchanged data should be carefully considered to avoid malfunctioning during normal operation or external faults. A comprehensive survey that covers the recently proposed unit protection schemes for VSC-HVDC grids will be presented in Section 4.

As compared to double-ended protection schemes, single-ended schemes are more economical (no need for communication channels) and faster (no communication delays) [68]. However, their level of selectivity is deteriorated particularly in the event of high-resistance faults [69]. Therefore, DC reactors, installed at both ends of each segment, are necessary to divide the entire grid into individual protection zones such that internal and external faults can be reliably discriminated. Moreover, precise and noise-free local measurements are necessary to guarantee the secure operation of such schemes. The various non-unit protection schemes and their principles will be discussed in Section 5.

3.2. Backup Protection Schemes

Backup protection schemes are not required to be as fast as primary protection schemes. Therefore, double-ended schemes can be employed to provide selective and reliable backup protection. Backup protection is essential to ensure power system protection in case of primary protection failure (due to relay or breaker failure). Several proposed single-ended

primary protection schemes have been augmented with double-ended backup criteria based on, e.g., the rate of change of voltage (ROCOV) at line terminals [70,71], the polarities of current variation at line terminals [72], and the boundary reactor voltage [73].

Other backup protection schemes have been proposed in the literature. For example, the algorithm introduced in [74] provides rapid backup protection to detect both local and remote breaker failures based on double-ended voltage and current measurements. In [75], a single-ended backup protection algorithm is proposed that discriminates between relay and breaker failures employing classifiers that are trained based on the K-Nearest Neighbor (KNN) approach using voltage and current measurements of the local breaker during the interruption process. In [76], a double-ended backup scheme is proposed based on detecting the direction of the reactive energy flow at both ends of the line, which is extracted by Hilbert-Huang Transform (HHT), in order to discriminate between internal and external faults. The pilot backup protection algorithm investigated in [77] is based on extracting the frequency characteristics of the DC filter output current by Discrete Fourier Transform (DFT) to estimate the specific frequency current values that are utilized to distinguish between internal and external faults. Finally, Ref. [78] proposes a unit backup protection scheme based on Wavelet Packet Energy Entropy (WPEE) of the transient fault currents at line terminals to provide reliable and selective backup detection of high-resistance pole-to-ground faults.

Comparing the aforementioned backup schemes, the single-ended scheme proposed in [75] has the minimum cost since it does not require communication channels, yet remote relay and breaker failures are not considered. In terms of speed, the proposed schemes in [74,75,78] have the minimum delay between the detection instant of the primary protection failure and the backup protection operation since primary protection failure is detected as early as possible by tracking the voltage and current variations during the primary breaker operation such that uncleared faults are rapidly detected. The proposed scheme in [77] has the lowest speed with an operating time up to 145 ms.

4. Double-Ended Schemes

Double-ended schemes can be categorized according to the exchanged information into two major groups, i.e., differential and directional. Differential schemes, similar to AC differential protection schemes, depend on exchanging information such as fault current measurements. Thus, they require high bandwidth communication channels and synchronized exchanged data. Aiming to enhance the speed of double-ended schemes, reduce the communication channel loading, and loosen the stringent synchronization requirements, logic (binary) data, representing the orientations or polarities of measurement quantities or specific extracted features from the measurements, are exchanged between the two ends of the protection zone in case of directional schemes such that selective, reliable, and fast unit protection algorithms with limited communication capacity are realized [79,80].

4.1. Differential Protection Schemes

Similar to AC differential protection schemes, DC differential schemes employ operating and restraining signals that are calculated based on the difference between and the average of boundary measurements, respectively. For instance, the principle of operation of current differential schemes is such that during normal operation or external faults, since measured currents at both ends of the protection zone have the same direction and approximately the same magnitudes, the differential current approaches zero. On the contrary, in the case of internal faults, the differential current will reach larger values. Therefore, by comparing the differential current with a non-zero threshold, to compensate for stray capacitive currents and other measurement errors, a reliable and selective fault indicator is achieved [81]. For example, current measurement information is exchanged between the two ends of the protection zone in the differential scheme introduced in [81], where the positive and negative pole currents at both ends of each segment are denoised using

Discrete Wavelet Transform (DWT). Then, their extracted energy contents are employed to form the operating and restraining signals of the proposed criterion. The ratios between the operating and restraining signals of each line are utilized to discriminate between internal and external faults and identify the faulty pole. The large data window (1000 samples) is required in this algorithm, which is continuously processed, and the heavy wavelet computations significantly delay the fault detection process.

In [82], fault-tolerant inductor-capacitor-inductor (LCL) VSCs, which can greatly limit fault currents for extended periods, are employed along with mechanical DCCBs such that a low-speed, yet highly-reliable and highly-selective protection system is realized based on a current differential protection criterion. However, the large operating time of the proposed algorithm (30–60 ms) may adversely impact the stability, security, and supply continuity of the overall transmission network. A similar scheme is proposed in [83] but with full-bridge MMCs exploiting their distinctive fault-handling capabilities such that slower and more cost-effective mechanical DCCBs with smaller ratings can be utilized. However, the enhanced control of these converters can substitute the need for DCCBs; thus, achieving improved speed at a much lower cost.

A fast differential algorithm has been recently proposed in [84] which realizes a compromise between selectivity and speed. Transmission lines are modeled by the approximated Bergeron model based on which the 1-mode components of the measured currents at boundary relays are rapidly computed. Then, their differential component is utilized to detect internal fault events. Although the Bergeron line model strengthens the immunity of the proposed scheme against malfunctioning during system disturbances and external faults, its precision needs further investigation considering the line distributed capacitances. A similar approach was proposed in [85], but applied only to point-to-point configurations. The backward traveling wave-based differential algorithm proposed in [86] utilizes Marti's frequency-dependent line model to exploit the implicit fault-transient high-frequency components. It can precisely detect and discriminate various DC faults, including faults that involve the metallic return path in asymmetric bipolar configurations, without using computationally intensive signal processing approaches. A voltage differential protection criterion is proposed in [87] based on the calculated differential-mode components considering the impact of the line frequency-dependent parameters. The improved algorithm does not require data synchronization for its effective operation since it can detect out-of-synchronization events and then resynchronize the mismatched information.

In summary, the common ground of the above differential protection schemes is that accurate, synchronized, and denoised current or voltage measurements have to be exchanged through an efficient communication medium to guarantee their reliable operation. In addition, the speed of the proposed algorithms does not necessarily comply with the stringent speed requirements recently imposed for multi-terminal HVDC grids [63].

4.2. Directional Protection Schemes

Compared to differential schemes, directional algorithms result in faster double-ended protection schemes that require communication channels with limited capacity. They vary based on the exchanged pilot signals, e.g., the directions of fault current measurements, the polarities of reactor voltages, and the signs of traveling waves transient energies. This section discusses various types of the proposed directional protection schemes.

4.2.1. Fault Current Direction

Digital signals that represent the direction of fault currents at the remote terminal can be utilized as pilot signals alongside local measurements for selective fault detection. Similar to AC systems, the developed scheme may be a tripping scheme (where the local tripping command will be initiated only if a fault confirmation signal is received from the remote end) or a blocking scheme (where the local tripping command will be initiated if a blocking signal from the remote end is not received). A tripping scheme is proposed in [88] based on exchanging the sign of fault current directions. It is concluded that an internal

fault is detected if the two terminal currents have the same sign, whereas opposite signs indicate an external fault. In [89], orientations of the transient fault currents at line ends are determined by the Wavelet Transform Modulus Maximum (WTMM) technique; then, they are communicated and compared with each other based on which internal and external faults are identified. However, the required large sampling frequency of 100 kHz increases the computational burden of this algorithm.

4.2.2. Boundary Reactor-Based Pilot Signals

Although DC boundary reactors are not required with double-ended schemes for grid segmentation, they may be utilized as current limiters to reduce the sharp rise of the fault current. In [90], the polarities of the boundary reactor voltages at both line ends are exchanged and compared to decide whether the detected fault is internal (positive polarities) or external (opposite polarities). In addition, the faulty pole is identified by integrating the reactor voltage over a data window to eliminate the coupling effect between the faulty and healthy poles. Likewise, transient properties of boundary reactor voltages are extracted by Wavelet transform in [91] based on which a pilot discrimination criterion is proposed.

4.2.3. Traveling Wave-Based Pilot Signals

During DC faults, traveling waves are initiated at the fault point, then propagate in both directions along the faulted segment until reaching the boundary terminals where one part of these waves is refracted into the healthy part of the grid and the other part is reflected into the faulted segment, and so forth [92]. Traveling wave-based algorithms are widely used to design unit and non-unit protection schemes. The permissive scheme designed in [79] classifies forward and reverse faults via calculating the energy content ratio of the fault incident backward wave over the reflected forward wave at boundary relays. Then, a permissive (or blocking) signal is sent to the other end to initiate (or prevent) the tripping signal of local DCCBs in case of forward (or reverse) faults.

To decrease communication delays and traveling wave attenuations in case of long cables, Reference [93] proposes a protection algorithm that utilizes multiple intelligent sensors located at cable joints and along the entire cable length. The proposed algorithm is based on a directional comparison criterion where a trip signal is initiated if two consecutive sensors detect a forward fault. Moreover, proactive (or two-stage) DCCBs [54], which discard the initial trip signal if the fault is not confirmed before the breaker opens, are employed to further reduce the total fault detection and clearing time. Therefore, the algorithm speed and security are greatly improved. However, the main deficiency of this scheme is the increased cost of the additional sensors.

Another pilot scheme is proposed in [94] based on comparing the orientations of transient energies (TEs) computed from the initial fault voltage traveling waves at both cable ends. The proposed algorithm effectively discriminates between internal (both TEs are negative) and external (one or two TEs are positive) faults. It also identifies the faulty pole based on the ratio between the computed TEs of positive and negative poles of the faulted segment. In addition, it estimates the fault location based on detecting the initial voltage surge arrival instants at both cable terminals, which are extracted by Stationary Wavelet Transform (SWT). However, the reliable performance of the proposed scheme requires substantial sampling frequency (1 MHz), which increases the computational burden. A similar algorithm based on TE is proposed in [95], where the propagation of current traveling waves and voltage measurements at boundary relays are used to estimate the TE values such that forward and backward faults are distinguished and the faulty pole is rapidly identified. In [96], the transient fault current increments in addition to their polarities at both line ends are evaluated and employed to discriminate between internal (opposite polarities) and external (same polarities) faults and precisely estimate the fault distance.

In [97,98], the phase-mode transformation is applied to bipolar DC cables resulting in six decomposed current and voltage components based on which multiple protection criteria are obtained. In [97], the high-frequency contents of the sixth mode current components are extracted employing the S-transform (which combines the advantages of Fourier and wavelet transforms). The proposed detection criterion is based on detecting the abrupt changes in the extracted high-frequency contents, while the fault discrimination criterion depends on comparing their polarities at cable ends. Finally, the extracted zero-frequency components are utilized to avoid malfunctioning in case of disturbances. Likewise, the proposed scheme in [98] utilizes the phase-mode transformation decoupling approach, applied to the forward and backward initial fault current traveling waves at cable ends, to calculate the fifth and sixth mode current components. Then, SWT is employed to estimate their amplitudes and polarities in order to be adopted in the fault discrimination and faulty-pole selection criteria.

4.2.4. Harmonic Current-Based Pilot Schemes

In such schemes, converters' harmonic currents at line terminals are extracted and analyzed to identify internal and external faults. In [99], first carrier frequency harmonic (FCFH) currents are extracted by DFT at cable ends. Based on their magnitudes during a certain window length, the protection units at both terminals detect internal faults and distinguish them from external faults. The proposed algorithm was only applied to point-to-point configurations and did not consider high-resistance faults. A similar, yet improved scheme is proposed in [100] based on FCFH currents extracted by HHT, which has several advantages over Fourier and wavelet transforms in terms of instantaneous frequency detection precision in the time domain. Furthermore, compared with the previous scheme, the algorithm was evaluated in a multi-terminal grid rather than a simple point-to-point configuration; besides, a larger range of fault resistances was tested. It is worth mentioning that harmonic-based schemes require high computation capacity and they are easily affected by noise and disturbances. Therefore, their sensitivity and selectivity may be endangered under particular fault scenarios.

4.2.5. Special Methodologies for Pilot Schemes

Recently, new mathematical approaches, which require lower computation capacity compared with conventional methods, are exploited to design fast and effective DC protection schemes. Morphological gradient theory is employed in [101] to develop the Multi-resolution Morphological Gradient (MMG) algorithm, which efficiently extracts the desired waveform information even during the loss of communication. In [101], MMG, which eliminates the errors resulting from data-synchronization mismatches, is applied to the line-mode voltage traveling waves. The proposed scheme discriminates between internal and external faults by estimating the correlation coefficient between the MMGs of line-mode voltage traveling waves at line terminals (the forward wave at one end and the backward wave at the other end). Finally, faulty pole identification is achieved based on calculating the ratio of MMG for the positive pole over that of the negative pole of the faulted segment. However, the operating time of this algorithm (5 ms) needs to be reduced to comply with the recent DC protection system speed requirements.

Cosine distance criterion is another recent approach proposed in [102]. This criterion is based on comparing the orientations of the reference internal fault voltages and currents with the corresponding orientations of the actual superimposed fault quantities via calculating the cosine distance function. Protection algorithms based on the Hausdorff Distance (HD) approach are proposed in [66,103]. The HD between two nonempty sets can be mathematically defined as the maximum distance of a set to the nearest point in the other set. The proposed methods in [66,103] provide major advantages in terms of noise-tolerance capability and elimination of the compulsory data synchronization requirement. The fundamental principle proposed in both algorithms is based on evaluating the degree of similarity, via HD theory, between the initial fault voltage backward and forward

traveling waves at line terminals (the forward wave at one terminal and the backward wave at the other terminal) to detect and discriminate between internal and external faults. Moreover, the faulty pole is identified in [103] based on the ratio of the transient energy of the positive pole over its counterpart of the negative pole. However, due to the relatively low speed of this scheme, it can be employed for backup protection rather than primary protection.

4.3. Comparison between Double-Ended Schemes

Table 4 presents a summarized comparison among a selected set of the reviewed schemes. The comparison is based on various aspects such as the exchanged data, mathematical approach, sampling frequency, and data window length based on which the algorithm can make decisions. Furthermore, the configuration of test grids and the converter technologies employed to evaluate the proposed schemes are provided. Moreover, the speed of the algorithms and their fault resistance coverage, beyond which the selective and reliable performance of the proposed algorithms will no longer be guaranteed, are compared. It is worth noting that the reported operation times of the algorithms depend on the propagation speed of the traveling waves and the communication time delay, which depends on the employed communication medium and the lengths of the overhead lines and/or cables within the test grid.

Based on Table 4, it is evident that differential schemes are generally slower than directional schemes. To the best of the authors' knowledge, the fastest differential algorithm is the one reported in [84] with an operating time of 7.5 ms, given that the longest transmission line within the test grid has a length of 800 km. However, this operating time is still large considering the recent protection system speed requirements. Furthermore, stringent synchronization requirements are mandatory to accurately estimate the differential current and avoid relay maloperation during severe external faults. On the contrary, directional schemes have shorter operating times, as they only require the exchange of binary signals with less stringent synchronization requirements. The minimum operating time of the reviewed directional schemes is 2.57 ms, which is reported in [94], given that the longest cable within the test grid is 200 km long. In addition, the fault resistance coverage of this scheme is 150 Ω , which is relatively small compared with other unit protection schemes. The largest fault resistance coverage is 1000 Ω , which is achieved by the proposed directional schemes in [93,101–103], while the lowest coverage is 100 Ω , as reported in [88,99].

Compared with differential schemes, directional schemes usually require a large sampling frequency and a high computation capacity. The directional scheme proposed in [94] has the largest sampling frequency of 1 MHz. In contrast, the lowest sampling frequency is 2 kHz, as reported in [88]; however, the fault resistance coverage of this algorithm is small and it is slow.

In summary, it can be concluded that communication-based schemes can attain a high level of selectivity since the multi-terminal grid is divided into separate protection zones at the boundary points where the information is exchanged; thus, the faulted segment can be reliably identified. Furthermore, recently proposed pilot schemes can comply with protection system speed requirements, particularly with short distances up to 200 km [94,102]; consequently, these algorithms can provide primary and backup protection. However, with longer transmission lines/cables and the imposed synchronization requirements, their utilization will be merely restricted to backup protection. Fiber-optic links are typically utilized by the reported schemes as the communication medium for exchanging data between boundary relays due to their high reliability and immunity against communication failures and erroneous data transmission. In addition, their large bandwidth facilitates the transmission of a large amount of data. Moreover, they are robust against electromagnetic interferences.

Table 4. Comparison among various communication-based protection schemes.

Ref. (Year) (Category)	Exchanged Data	Mathematical Analysis Tool	Algorithm Triggering Criterion	Sampling Frequency (kHz)	Window Length (Number of Samples)	Tested Grid Configuration	Converter Topology	Fault Resistance Coverage	Operation Time (ms)
[81] (2016) (differential)	Current measurements	DWT	High-frequency transients	100	1000	Three-terminal star-connected	Three-level NPC-VSC	300 Ω	10
[82] (2015) (differential)	Current measurements	Direct data processing	Differential current	10	Instantaneous measures	Four-terminal meshed grid	Two-level LCL-VSC	N/A	30–60
[83] (2018) (differential)	Current measurements	Direct data processing	Differential current	N/A	Instantaneous measures	CIGRE test grid	Full-bridge MMC	400 Ω	20
[84] (2021) (differential)	Current measurements	Phase modal transformation	Differential current (1-mode)	10	Instantaneous measures	Three-terminal star-connected	LCC/MMC (hybrid)	500 Ω	7.5
[88] (2013) (directional)	Current polarity	Direct data processing	Current direction change	2	10	point-to-point	Two-level VSC	100 Ω	10
[90] (2019) (directional)	Reactor voltage polarity	Phase modal transformation	Reactor voltage gradient	50	25	Four-terminal meshed grid	Half-bridge MMC	400 Ω	3
[89] (2018) (directional)	Fault current direction	WTMM	Same as the main algorithm	100	Instantaneous measures	Four-terminal meshed grid	Two-level VSC	300 Ω	3
[93] (2018) (directional)	Fault current direction	Direct data processing	Voltage/current variations	N/A	Instantaneous measures	Four-terminal meshed grid	Half-bridge MMC	1000 Ω	5
[94] (2018) (directional)	TE polarity	Integration of wave power	Abrupt voltage variations	1000	500	Four-terminal meshed grid	Half-bridge MMC	150 Ω	2.57
[96] (2021) (directional)	Current polarity	Direct data processing	Abrupt current variations	20	Instantaneous measures	Point-to-point	Half-bridge MMC	300 Ω	N/A
[99] (2014) (directional)	FCFH current detection flag	DFT	Same as the main algorithm	N/A	27	Point-to-point	Two-level VSC	100 Ω	N/A
[100] (2019) (directional)	FCFH current detection flag	HHT	Same as the main algorithm	100	512	CIGRE test grid	Two-level/three- level VSC	500 Ω	N/A
[101] (2021) (directional)	Line mode voltage	MMG	MMG value	10	31	Four-terminal meshed grid	Half-bridge MMC	1000 Ω	5
[102] (2021) (directional)	Fault detection signal	Cosine distance function	Same as the main algorithm	5	10	Four-terminal meshed grid	Half-bridge MMC	1000 Ω	3
[103] (2021) (directional)	Forward and backward voltage waves	Improved HD hypothesis	Instantaneous frequency obtained from HHT	20	40	Four-terminal meshed grid	Half-bridge MMC	1000 Ω	7.22

5. Single-Ended Schemes

Double-ended schemes are mostly slow due to the inevitable communication delays, which become longer as the transmission line or cable length increases. Furthermore, various errors in the exchanged data may occur due to noise and loss of synchronization. Consequently, unit schemes are practically recommended to provide reliable backup protection. Non-unit protection algorithms, which depend merely on local measurements, are required to provide fast primary protection. The main challenge that hinders the design of single-ended schemes is achieving high selectivity, especially in the case of remote faults with large resistances. Furthermore, to guarantee high accuracy, a large sampling frequency is commonly required, which increases the algorithm's computational burden. Additionally, attenuation of traveling waves associated with long transmission lines should be carefully considered to avoid the maloperation of the designed algorithms [104]. Various approaches and methodologies have been proposed to design selective, sensitive, and reliable non-unit protection schemes that will be reviewed in this section.

5.1. Voltage Derivative-Based Schemes

One of the earliest approaches that has been adopted to design non-unit protection schemes is based on the continuous computation of the ROCOV values based on local voltage measurements. Since DC faults are accompanied by a rapid voltage decline, the ROCOV value can be exploited to detect fault events. However, these schemes require large sampling frequencies to accurately calculate the ROCOV value. Additionally, their selectivity is endangered in case of high-resistance faults. For instance, the proposed scheme in [105] depends on the local line-side reactor voltage measurements to estimate the ROCOV value that is compared to a pre-adjusted threshold for DC fault detection and localization. A comparable scheme is proposed in [106], which is equipped with an additional overcurrent criterion to increase the fault resistance coverage.

The authors of [70,71] have further improved the selectivity, reliability, and fault resistance coverage of the ROCOV scheme by proposing an extra directional feature based on the ratio of ROCOV values measured at both sides of the boundary reactors. In addition, the proposed scheme is augmented with a directional comparison ROCOV-based criterion to selectively detect high-resistance faults. This directional criterion has been further improved in bipolar grids with a metallic return path via inserting small reactors at the return conductor ends in [71]. In [107], a double-stage scheme is proposed. In the first stage, fault is detected based on undervoltage criterion, while the second stage is the discrimination stage based on an undervoltage and voltage derivative criterion to discriminate between internal and external forward faults as well as a current derivative criterion to identify forward faults from reverse faults. Furthermore, the concept of applying a reduced grid model to accurately determine the algorithm thresholds is introduced.

5.2. Current Derivative-Based Schemes

Analogous to voltage derivative-based schemes, current derivative-based schemes have been proposed, in which the instantaneous increase of fault current and the rate of change of current (ROCOC) are utilized to detect fault events. The ROCOC can be integrated with other criterion to develop selective algorithms and improve the algorithm reliability and immunity against maloperations. In [108], five ROCOC indices are calculated based on which various faults are detected (including faults that involve the metallic return conductor in asymmetric bipolar configurations) and the faulty pole is identified as well. Another ROCOC-based scheme is proposed in [109], which provides both primary and backup protection for multi-terminal HVDC grids. In [109], a statistical Bayesian classifier is adopted to select the necessary thresholds and establish a proper time-coordination between primary and backup relays.

5.3. Transient Schemes Based on Voltage and Current Measurements

DC fault events are associated with a abrupt increase in the fault current and sudden dips in the voltage. Therefore, direct measurements of local voltages and currents can provide fault indicators and can be employed in the design of rapid fault detection algorithms. It is worth noting that reliable voltage and current measurement devices with a high bandwidth should be utilized in order to provide precise and noise-free measurements based on which correct decisions can be made by the proposed algorithms [110]. For instance, a transient-based protection scheme applicable to MMC-HVDC grids with unidirectional solid-state DCCBs is proposed in [111] based on three criteria, i.e., overcurrent, undervoltage, and ROCOC. In [21], the proposed criterion depends on transient voltage measurements at both sides of the terminal reactors. In [21], the ratio of the transient voltages (ROTV) at reactor ends is used to distinguish between internal and external faults. In [112], fault detection and identification (FDI) units are arranged at each bus to promptly detect faults, discriminate between bus and line faults, and selectively identify the faulted line or busbar based on local transient current measurements. A similar scheme is proposed in [113]. A general analytical criterion for threshold estimation is proposed in [104], which is capable of determining transient voltage-based algorithms' thresholds in a systematic way and without requiring extensive simulations.

The non-unit differential criterion established in [114] depends on transient current measurements obtained from distributed fiber-optic current sensors along the protected lines in order to precisely identify the faulted segment. The proposed local differential criterion in [115] detects and discriminates between internal and external faults after computing the ratio between the transverse differential (cross difference) currents and the sum of the locally-measured fault currents of both positive and negative poles. Although the proposed scheme cannot be directly applied as a stand-alone primary protection algorithm, it can be utilized as either auxiliary primary protection or backup protection. In [116], the proposed criterion depends on cable sheath voltage measurement, which is typically zero during normal operation while having a non-zero value during the fault. Furthermore, in [116], the amplitude and polarity of the measured sheath voltage are utilized to identify the faulted segment and determine the faulty pole. In [117], the rate of change of the current-to-voltage ratio, i.e., conductance derivative of the local transient voltage and current measurements, is employed to detect fault events. The proposed scheme in [118] utilizes the transient fault voltage measurements to estimate the first peak time (FPT), which represents the time duration between the sudden voltage decline instant and when the first peak is detected in the filtered voltage waveform, based on which the protection criterion is established. In [119], the change in the average voltage of positive and negative poles is employed to selectively detect various fault events. However, the employed measurement data window length is large (5 ms).

In [120], the magnitudes and derivatives of the common-mode (CM) and differential-mode (DM) components of the local fault current are extracted based on modulus decomposition transformation. Then, the extracted values are projected on a protection phase plane, which is divided into fault regions according to the fault type. Consequently, internal faults can be detected and discriminated from external faults, and the faulted pole can be identified as well. The proposed scheme in [121] utilizes the local fault voltage and current measurements to estimate three independent fault indicators, i.e., pole-current variations, pole-to-earth voltage variations, and converter neutral current variations, based on which different faults can be detected. In [122,123], initial fault currents are analyzed and calculated by proposing a transient high-frequency equivalent model for the employed meshed grid. Next, a fault detection and discrimination criterion is proposed based on estimating the transient energy of the superimposed high-frequency components of the local current measurements [122]. In [123], the derived current expressions during the initial fault stage are used to detect and discriminate between internal and external faults.

5.4. Boundary Reactor-Based Schemes

As previously highlighted in Section 2.1, DC reactors are installed at both ends of the transmission line or cable segments in HVDC grids not only to limit the sharp increase of fault currents but also to divide the grid into separate protection zones. Various protection schemes based on boundary reactor measurements have been proposed in the literature. In [72], the estimated value of the limiting reactor power is utilized to detect and discriminate between internal and external faults. However, the proposed scheme is not reliable in detecting high-resistance faults. Therefore, an auxiliary pilot backup criterion is developed for such faults. In [73], the proposed criterion depends on voltage measurements across the boundary reactors to detect and discriminate various faults and identify the faulty pole. Depending on the rate of change of the reactor voltage measurements, the proposed scheme in [124] detects fault events. Besides, internal faults are discriminated from external faults depending on the voltage polarities and amplitudes of the reactors that are connected to the same bus. However, in [124], only pole-to-pole faults are tested without providing a faulty-pole identification criterion. In [125], the proposed algorithm detects DC faults by calculating the difference between the ratios of the root mean square values of transient voltages (DTRVs) at both sides of the boundary reactor. Moreover, the faulted pole is identified by calculating the instantaneous zero-sequence voltage (IZSV) at the converter AC-side. The concept of asymmetric pole inductors has been recently proposed in [126], where the value of the DC reactor installed at the positive pole is different from that of the negative pole. The difference between the inductor voltages of the two poles is utilized as the fault detection criterion. However, this scheme is incapable of detecting unsymmetrical DC faults, i.e., pole-to-ground faults.

5.5. Traveling Wave-Based Schemes

Similar to double-ended schemes, traveling wave propagation theory has been widely applied in the design of single-ended schemes. In such schemes, fault-induced traveling waves are detected and their high-frequency contents and arrival instants are extracted by utilizing various signal processing tools based on which DC faults are detected. However, the impacts of the superimposed noises and wave attenuations in case of long distances should be minimized to guarantee the reliable performance of these protection schemes. For example, DWT applied to local fault voltage traveling waves is exploited in [127] to identify the faulted segment. In [128], DWT is applied to local fault current measurements to design the protection criterion, where the fault discrimination is achieved by detecting the high-frequency components that exist during internal faults. In case of external faults, these components are attenuated due to the shunt capacitors installed at the grid tie buses and the stray capacitances at each bus. The proposed discrimination criterion employs the ratio of the high- to low-frequency transient energies to distinguish between internal and external faults. However, the proposed scheme lacks generalization since it is tested in a special grid structure that contains tie buses. In [129], DWT is applied to local voltage measurements to detect various faults where the faulted line is identified based on integrating the square of the transient voltage, i.e., transient energy. Moreover, the faulted pole is discriminated based on tracking the change of the positive and negative poles' transient voltages. The proposed scheme in [130] locally extracts the distinctive frequency contents of the first incident traveling wave of the fault current utilizing DWT to distinguish between internal and external faults. In [131], DWT is used to extract the high-frequency components of the line-mode voltages and currents of the fault induced forward and backward traveling waves to discriminate between forward and reverse faults.

A multi-criteria wavelet-based scheme is proposed in [22], where the proposed algorithm utilizes two out of three criteria (voltage wavelet coefficients, current wavelet coefficients, and local voltage magnitude and derivative) to reliably detect various faults. Moreover, each criterion consists of a fault detection stage based on voltage and current measurements and a fault localization stage based on the comparison between the wavelet coefficients of each cable within the grid. The proposed scheme in [132] is based on ex-

tracting the dominant frequency component of the local current measurements using the multiple signal classification (MUSIC) approach. Furthermore, transient wave energy calculated by wavelet transform is utilized to discriminate between far-end internal and external faults, while WTMM is applied to identify the faulty pole. In [133], the proposed fault detection and discrimination criterion is based on the Synchrosqueezing Wavelet Transform (SWT) applied to the measured voltage signals across the boundary reactors.

Fourier transform is employed in [23] to extract the high-frequency components of the local current measurements, which have different features in the case of internal and external faults. In [134], the high-frequency content extraction is performed by Short Time Fourier Transform (STFT) applied to local fault current measurements to develop a frequency-domain-based relaying algorithm. Moreover, a time-domain-based detection criterion is proposed based on estimating the correlation degree between the DC link capacitor discharge current and the local fault current. Fast Fourier Transform (FFT) is employed in the protective scheme proposed in [135]. In [136], the orientations and the high-frequency content of the initial fault current traveling wave extracted by FFT are utilized to construct the fault detection and identification criteria. However, the proposed method requires a large sampling frequency and high computation capacity.

Recently, HHT has been used in several protection schemes due to its capability of extracting instantaneous features with a physical meaning in the time-domain [137]. For instance, in [138], the average frequency of the transient voltage signal is estimated by HHT and the marginal Hilbert spectrum (MHS). Then, the estimated value is compared with a predefined distance-frequency curve to assess the fault location. However, this scheme requires extensive calculations to find the distance-frequency curve for each segment within the grid. In addition, the selectivity of this scheme is examined only for low-resistance (1Ω) faults. In [139], the instantaneous energy density, estimated by HHT, is selected as the fault detection criterion. However, the frequency band, within which the density level is estimated, depends on the operating point of the system. Moreover, the fault resistance coverage of this scheme is relatively small (50Ω).

In [140], a protection algorithm is proposed based on the zero- and line-mode components of the fault backward traveling waves extracted by Phase-Modal Transformation (PMT). Similarly, PMT is employed in [141], where internal faults are detected by using the line-mode components of the boundary reactor voltage and the faulty pole is identified based on the zero-mode components. In [142], likewise, a PMT-based algorithm is proposed, which uses two criteria to detect fault events: (1) the derivative of the line-mode forward traveling wave and (2) a directional criterion based on the surge arrival time difference (SATD) between the line-mode components of backward and forward traveling waves. In [143], depending on the local fault voltage and current measurements, a parametric model is developed, which extracts the transients of the fault voltage and current traveling waves to detect various fault events based on an iterative maximum-likelihood (ML) approach.

5.6. Distance Protection-Based Schemes

Distance protection concept is adopted in [144,145]. In [144,145], the accurate frequency-dependent line model is employed. Based on the local voltage and current measurements, the fault distance is precisely estimated by solving a set of line differential equations. A similar approach is proposed in [146], where the lumped π -model of the line is utilized. The probe capacitors are inserted at the DC-side of each grid terminal in [147]; then, based on the estimated resonance frequency (by least-squares technique) between the added capacitors and grid inductances, internal and external faults are distinguished. Finally, in [148], a distance algorithm is proposed based on estimating the equivalent capacitance voltages (ECV) of half-bridge MMCs and tracing their polarity.

5.7. Artificial Intelligence-Based Schemes

Various artificial neural network (ANN)-based protection schemes have been proposed, which benefit from intelligent fault detectors and classifiers. In [149], an ANN-based scheme depending on local fault current measurements is proposed. However, this scheme has a long operating time of 5 ms. The proposed scheme in [150] uses a feed-forward ANN to extract the energy involved in the current signal spectrum at two distinct frequency bands for fault detection. In [151], wavelet transform along with Principal Component Analysis (PCA) are applied to the local current measurements to extract distinctive features, which are utilized as inputs to a Genetic Fuzzy System (GFS) to discriminate between internal and external faults. Furthermore, in [152], an artificial intelligence-based discrimination criterion is proposed based on the fault induced initial traveling wave propagation features extracted by a convolutional neural network (CNN). It is worth mentioning that artificial intelligence-based schemes require high computation capacity, exhaustive simulations, and large data sets to train the algorithms.

5.8. Special Non-Unit Schemes

Recently, various mathematical approaches have been used to design efficient single-ended protection algorithms. The authors of [153] have developed a non-unit protective scheme based on the Morphological Gradient (MG) theory. In [153], the MG theory is used to extract the amplitude and the arrival instant of the initial fault wavefront of the local voltage to detect fault events. In [154], this scheme is modified based on the multiplication of the estimated second-level MG values of the line-mode components of the fault voltage and current traveling waves. The proposed scheme in [155] depends on detecting the sudden changes of the transients associated with the local fault voltage and current traveling waves using the Median Absolute Deviation (MAD) statistical approach.

In [156,157], the Levenberg-Marquart (LM) curve fitting technique is applied to the zero-mode component of the first incident traveling wave of the measured fault current to extract the index coefficients, which are utilized to distinguish internal from external faults. A similar scheme is developed in [158], where the fault resistance and location are respectively estimated based on the magnitude and the distortion degree of the incident fault current traveling wave. Moreover, in [158], the effect of the fault resistance is eliminated by utilizing adaptive thresholds, which are adjusted based on the extracted fault information from a curve fitting criterion. Although the proposed scheme can reliably identify pole-to-ground faults with large fault resistances, it fails to detect pole-to-pole faults. Furthermore, it requires a large sampling frequency and a large computation capacity. Finally, a recent algorithm is proposed in [159] based on the statistical random matrix theory (RMT) applied to local current measurements. This algorithm detects faults with a large range of resistances.

5.9. Bus Protection Schemes

Protection schemes are required to reliably detect bus faults and discriminate them from line faults. Bus faults will result in tripping not only the associated converter station but also all the connected lines. Therefore, bus protection algorithms must not maloperate in the case of line faults and other transients. The fundamental bus protection criterion is based on Kirchhoff's Current Law (KCL), where the infeed current into the bus from the converter station must be equal to the summation of the outgoing currents in the connected lines. The current differential criterion based on KCL has been widely adopted in the literature [112,127]. Furthermore, a ROCOV-based criterion is proposed in [70,71] to detect bus faults. In [160], the cosine distance criterion is employed to design a non-differential bus protection algorithm based on the bus voltage and the direction of the superimposed fault currents of the lines connected to the protected bus.

5.10. Comparison between Single-Ended Schemes

A comparison between single-ended schemes is presented in Table 5. The same comparison aspects as those used for double-ended schemes are investigated in addition to the size of the boundary reactors employed in the proposed schemes to ensure selectivity and limit the sharp rise of fault currents. From Table 5, it can be concluded that non-unit schemes are fast with operating times less than 1 ms [71,136]. The algorithm proposed in [155] has the longest operation time of 3 ms, which still complies with the protection system speed requirements and it has the smallest sampling frequency of 10 kHz. The largest sampling frequency (2 MHz) and the largest window length (1000 samples) are associated with the FFT-based scheme proposed in [136].

There are three significant aspects that should be carefully considered while evaluating the performance of single-ended schemes. First, the fault resistance coverage of the proposed schemes should be large enough such that severe fault conditions can be detected. The maximum fault resistance coverage is 800 Ω , which is achieved by the proposed scheme in [142]. In contrast, only faults with 1 Ω resistance are simulated in the proposed scheme in [138]. Second, the size of boundary reactors should be optimized, since large reactors may result in severe stability issues, particularly with power flow reversal, which is common in multi-terminal grids. Small reactors are superior in terms of stability and cost; yet their role in damping the sharp rise of fault currents may be seriously impacted. In [142], large reactor sizes in the range of 200–300 mH are employed to achieve the large resistance coverage of 800 Ω . The lowest reported reactor size is 5 mH, which is tested with the proposed scheme in [72]. Third, severe solid external faults such as solid local and remote bus faults should be evaluated and the proposed algorithms should be able to discriminate these faults from high-resistance internal faults. Note that this aspect may also affect the selection process of reactor sizes according to the required filtering level that guarantees successful discrimination between these critical faults.

Comparing unit schemes (Table 4) with non-unit schemes (Table 5), it is evident that non-unit schemes have relatively higher sampling frequencies and less fault resistance coverage compared with unit schemes. However, non-unit schemes are faster than unit schemes, mainly due to the exclusive dependency on local measurements and, thus, the absence of communication delays. Furthermore, non-unit schemes are more accurate, as they do not rely on communicated data; thus, they are not affected by communication and synchronization errors. In summary, there is a trade-off between selectivity and speed in single- and double-ended schemes. Based on the aforementioned discussions in Sections 4 and 5, selective single-ended schemes are the appropriate candidates for primary protection, whilst double-ended schemes should be employed as reliable backup protection algorithms. Furthermore, an exemplary single-ended scheme should be augmented with a powerful mathematical tool capable of rapidly extracting the internal fault signature under severe fault conditions. Although relatively fast unit schemes have been proposed in the literature, the unavoidable communication delays as well as data synchronization and incidental communication failures are the major impediments that endanger their reliable operation for primary protection.

Table 5. Comparison among communication-less protection schemes.

Ref. (Year) (Category)	Mathematical Analysis Tool	Algorithm Triggering Criterion	Sampling Frequency (KHz)	Window Length (Number of Samples)	Tested Grid Configuration	Converter Topology	Boundary Reactor Size (mH)	Fault Resistance Coverage	Operation Time (ms)
[105] (2016) (ROCOV)	Direct data processing	Same as the main algorithm	N/A	N/A	Three-terminal star-connected	Generic multilevel VSC	100	N/A	N/A
[71] (2018) (ROCOV)	Direct data processing	Same as the main algorithm	25	N/A	Three-terminal meshed grid	Half-bridge MMC	40	200 Ω	0.2
[107] (2016) (RO- COV/ROCOC)	Direct data processing	Undervoltage	100	10	Four-terminal meshed grid	Half-bridge MMC	20–40	60 Ω	2.11
[108] (2020) (ROCOC)	Direct data processing	Same as the main algorithm	N/A	N/A	Three-terminal star-connected	Half-bridge MMC	40	50 Ω	1
[21] (2017) (Transient)	Butterworth band-pass filter	Voltage derivative	50	50	Five-terminal meshed grid	Two-level VSC	10	300 Ω	1
[112] (2017) (Transient)	Direct data processing	Same as the main algorithm	50	20	Four-terminal meshed grid	Half-bridge MMC	50	N/A	0.5
[72] (2020) (DC Reactor)	Direct data processing	Same as the main algorithm	N/A	N/A	Point-to-point	two-level VSC	5–145	N/A	2.6
[73] (2018) (DC Reactor)	Direct data processing	DC reactor overvoltage	N/A	N/A	Four-terminal meshed grid	Half-bridge MMC	150	380 Ω	1
[127] (2018) (Traveling Wave)	DWT	Current variation	96	10	Five-terminal meshed grid	Half-bridge MMC	150	500 Ω	1
[136] (2020) (Traveling Wave)	FFT	Same as the main algorithm	2000	1000	CIGRE test grid	Half-bridge MMC	N/A	200 Ω	0.5
[141] (2020) (Traveling Wave)	PMT	Voltage derivative	N/A	N/A	Four-terminal meshed grid	Half-bridge MMC	150	200 Ω	1.1
[142] (2021) (Traveling Wave)	PMT	Voltage gradient	20	6	Four-terminal meshed grid	Half-bridge MMC	200–300	800 Ω	1
[154] (2021) (Special)	PMT/MG	Undervoltage	20	N/A	Four-terminal meshed grid	Half-bridge MMC	50	300 Ω	0.6
[155] (2021) (Special)	MAD	Same as the main algorithm	10	50	Four-terminal meshed grid	LCL Half-bridge MMC	20	N/A	3
[158] (2020) (Special)	PMT/BBF (basic fitting function)	Same as the main algorithm	200	200	Four-terminal meshed grid	Half-bridge MMC	100	300 Ω	1

6. Fault Location Identification Schemes

Precise determination of the fault location within the identified faulted segment is extremely important for rapid repair and fast restoration of the system. Similar to primary protection schemes, fault location schemes can be implemented with and without communication channels. In communication-based fault location identification schemes, the arrival instants of the first incident fault-induced backward traveling waves at both terminals of a transmission line or cable segment are obtained by means of signal processing tools to calculate the exact fault distance. However, synchronized measurements are essential to guarantee the accuracy of the proposed scheme. In addition, the parameters of the transmission link and its wave propagation characteristics should be carefully considered. For example, the proposed formula in [81] estimates the fault distance based on the arrival instants of the incident traveling waves, synchronized by the global positioning system (GPS), at boundary relays.

Likewise, Continuous Wavelet Transform (CWT) is employed in [161] to extract the wavefront arrival instants of terminal voltage measurements. In [162], the criterion is modified to be applicable to multi-terminal star-connected grids. The proposed scheme in [163] utilizes synchronized measurements of both conductor and sheath currents in order to estimate the fault distance in submarine cables.

Fast fault location identification schemes can be implemented based on local measurements without the need for synchronized exchanged data. The fundamental principle of these schemes depends on the detection of the arrival instants of the first two fault induced traveling waves [164]. Moreover, DC reactors play an integral role in the reliable operation of such schemes by filtering out the high-frequency components of the refracted traveling waves coming from neighboring segments. Robust signal processing tools are used in a number of algorithms to discriminate between the reflected traveling wave from the fault location and the one reflected from the remote terminal. For instance, the proposed scheme in [165] depends on detecting the arrival instants of both the initial and the subsequent reflected voltage traveling wave heads utilizing the Singular Value Decomposition (SVD) approach. Further, to mitigate the effect of measurement noises, Stationary Wavelet Transform (SWT) is employed to denoise the local voltage measurement signals. The proposed fault location identification scheme in [166] estimates the line impedance between the relay location and the fault point based on analyzing the local voltage and current measurements during the initial fault stage.

In [167], a pattern recognition-based scheme is proposed, which is based on estimating the Pearson correlation coefficient that measures the level of similarity between the local voltage signals and prespecified training patterns. The proposed scheme in [168] depends on the arrival instant of the first traveling wave extracted from local measurements without the need to detect the arrival instants of subsequent surges. In [168], the grid is divided into a number of sections and their corresponding set of linear equations is solved to accurately identify the fault location. Other single-ended fault location schemes have been recently proposed such as the Variational Mode Decomposition-based scheme [169], the characteristic impedance-based scheme [170], the high-frequency content-based scheme (extracted by the Lomb-Scargle Periodogram approach) [171], the estimated wavefront speed-based scheme [172], and HHT-based schemes [173,174].

7. Reclosing Strategies

A supplementary feature of protective algorithms is the capability to discriminate between permanent and temporary faults and to provide adaptive reclosing in case of temporary faults. Temporary faults are common in overhead transmission lines due to lightning strikes and their vulnerability to severe weather conditions, as previously indicated in Table 3. Reclosing strategies play an integral role in enhancing the stability and security of transmission networks by minimizing the outage duration in addition to guaranteeing the continuity of supply after fault extinction. In comparison with AC single-phase auto-reclosing (SPAR) schemes, DC reclosing schemes are more challenging

due to the weak coupling between the tripped pole and the healthy pole, in case of pole-to-ground faults. Thus, detecting the arc extinction instant of temporary faults is challenging. Therefore, fixed reclosing times with the option of multiple reclosures is the common practice used in DC reclosing schemes [175]. However, the multi-branch structure of DCCBs and their residual DC current breakers (as shown in Figure 10) can effectively facilitate the discrimination process through injecting testing signals by reclosing the residual breaker. Then, based on analyzing these signals, the fault nature (permanent or temporary) can be identified.

Various reclosing strategies have been proposed in the literature. In [176], a reclosing strategy for mechanical DCCBs is proposed based on transient operating voltages (TOVs), produced during fault interruption, which are used to distinguish between permanent and temporary faults and estimate the fault extinction instant in case of temporary faults. In [177], the DC component of the residual voltage generated after reclosing the residual breaker is used as an adaptive classifier to identify the fault nature. A similar approach is proposed in [178] based on residual voltage measurements, but it is applied to hybrid DCCBs rather than mechanical DCCBs.

Reclosing strategies based on active pulse injection and hybrid DCCBs are proposed in [179–182]. The proposed reclosing scheme in [179] is based on the injection of an active voltage pulse into the faulted line from the grid converters. Then, an undervoltage criterion applied to the refracted traveling wave is utilized to identify the fault property. Furthermore, to provide a path for the injected pulse, a coordinated control of hybrid DCCBs is required to conduct the transfer branch for a short time (0.1 ms). A similar scheme is proposed in [180] and based on a traveling wave criterion. In [181], the reclosing scheme is based on injecting voltage signals into the faulted lines. Then, a WTMM-based criterion is applied to the reflected traveling wave to distinguish between permanent and temporary faults. A similar scheme is proposed in [182] based on the injection of current traveling waves and the stored energy of the snubber capacitors of hybrid DCCBs.

Further research on reclosing strategies needs to be conducted in order to achieve prompt and reliable discrimination between permanent and temporary faults under severe fault conditions. Furthermore, enhancing the adaptive feature of the reclosing schemes such that they can precisely detect the extinction (deionization) instant of transient fault arcs in case of temporary faults is a current research challenge that requires further investigation.

8. Design Procedures and Standardization of HVDC Protection Schemes

The procedure to design a reliable HVDC grid protection systems and determine the various grid parameters and equipment ratings involves multiple crucial steps. In [183], a six-step procedure is introduced to design the protection system: (1) the appropriate HVDC grid topology (symmetrical, asymmetrical monopolar or bipolar configuration, with ground or metallic return path) is selected; (2) DC fault analysis and fault current calculations are performed to determine the short-circuit levels; (3) the proper fault clearing strategy is decided based on the desired performance requirements and grid limitations; (4) the required switchgear equipment and their ratings are determined; (5) the size of DC reactors is determined; and (6) the protection algorithm is designed. A significant aspect in the design of protection algorithms is the employed domain where the algorithm inputs are processed. As concluded in [184], the phase-domain is the preferred choice when designing a protection algorithm for cable-based HVDC grids, whereas the modal-domain is the best choice in overhead line-based HVDC grids.

Within the same context, optimal power flow (OPF) calculations are performed in [185] to select the appropriate HVDC grid topology in order to minimize fault transients and network losses. Furthermore, in [186], an optimal approach to design a reliable HVDC protection system is proposed where the design procedure is converted into an optimization problem solved using genetic algorithm. In [186], the desired protection aspects are considered as the problem objective functions such as minimizing the size of DC reactors. In addition, the system requirements and design parameters, e.g., protection margins,

thresholds, DCCB ratings, and the algorithm speed that prevents the blocking of converters during faults, are considered as the optimization problem constraints and variables.

Standardization of protection systems of HVDC grids is imperative to guarantee their secure operation. A pre-standardization study is presented in [187], where basic operational guidelines for realizing multi-terminal multi-vendor HVDC grids are outlined. Comprehensive standards for protection requirements, philosophies, and selection of fault interruption devices must be developed based on practical experiences with existing systems. Given the lack of large installed HVDC grids, protection standardization is still in its preliminary stage with various recommendations provided based on intensive analysis and simulations [188]. For instance, as recommended by the CIGRE Working Group (WG) B4.56, the acting speed of HVDC protection systems should be less than 10 ms in order to retain the stability of the HVDC grid during various fault events [189].

Other valuable CIGRE technical brochures, which outline significant recommendations regarding HVDC grid protection systems, were published in the preceding years, such as: (1) CIGRE Technical Brochure 739 [52], which outlines the practical recommendations and the available protection approaches and philosophies in order to realize effective protection schemes for meshed HVDC grids; (2) CIGRE Technical Brochure 683 [190], which demonstrates the HVDC protection system switchgear and the available DCCB technologies with their practical specifications; (3) CIGRE Technical Brochure 604 [191], which provides practical guidelines for modeling HVDC converters and other system elements in addition to a full description of the widely used CIGRE multi-terminal HVDC test system. The technical reports and brochures developed by regulatory organizations such as CIGRE have established the fundamental practices and recommendations based on which comprehensive standards for HVDC grid protection schemes can be fully instituted.

9. Conclusions

A comprehensive survey of HVDC grid protection systems has been presented in this paper. In this paper, the DC fault phenomenon including the fault stages, calculation methods, and fault clearing strategies are presented; in addition, various HVDC protection system requirements, which ensure the reliable performance of protection systems under severe fault conditions, are discussed. Furthermore, a comprehensive review of primary and backup protection algorithms is provided and the major differences between single- and double-ended primary schemes are addressed. Moreover, a comprehensive review of double-ended and single-ended schemes is presented. An overview of fault location identification schemes is provided; in addition, reclosing schemes in HVDC grids are reviewed. HVDC protection system design procedures and the available standards related to HVDC grid protection are also reviewed in this paper.

Based on the reviewed papers, a reliable and inclusive protection system for multi-terminal HVDC grids should possess the following features or components: (1) a selective primary protection algorithm that is able to rapidly detect various DC fault events and discriminate between internal and external faults with a low sampling frequency and limited computation requirements; (2) the ability to detect the faulted segment and precisely estimate the fault location in addition to identifying the faulty pole in the case of pole-to-ground faults; (3) guaranteed and reliable performance under severe fault conditions and different grid configurations; (4) the ability to detect bus faults and distinguish them from nearby internal faults; (5) a backup protection algorithm that provides delayed protection in the case of primary protection failure; and (6) a reclosing scheme that can distinguish between permanent and temporary faults in addition to determining the exact extinction instants of temporary fault arcs; thus, providing adaptive reclosing times to accomplish optimal network restoration.

Based on the presented review of the proposed protection algorithms, it can be concluded that there is a trade-off between selectivity and speed in single- and double-ended protection schemes. Highly-selective single-ended schemes are the appropriate candidates for providing primary protection given that they should be augmented with a powerful

signal processing tool capable of rapidly extracting the internal fault signature under severe fault conditions. On the other hand, double-ended protection schemes can be employed as reliable backup protection algorithms. The inevitable communication delays as well as data synchronization and incidental communication failures impede the use of double-ended schemes in providing primary protection.

Author Contributions: Conceptualization, M.R. and S.P.A.; methodology, M.R. and S.P.A.; software, M.R.; formal analysis, M.R.; investigation, M.R.; resources, M.R.; data curation, M.R.; writing—original draft preparation, M.R.; writing—review and editing, S.P.A.; visualization, M.R. and S.P.A.; supervision, S.P.A.; project administration, S.P.A.; funding acquisition, S.P.A. All authors have read and agreed to the published version of the manuscript.

Funding: This research was funded by a Discovery Grant provided by the Natural Sciences and Engineering Research Council (NSERC) of Canada and an Ontario Graduate Scholarship (OGS) provided by the provincial Government of Ontario, Canada.

Institutional Review Board Statement: Not applicable.

Informed Consent Statement: Not applicable.

Data Availability Statement: Not applicable.

Conflicts of Interest: The authors declare no conflict of interest.

References

1. Van Hertem, D.; Ghandhari, M. Multi-terminal VSC HVDC for the European supergrid: Obstacles. *Renew. Sustain. Energy Rev.* **2010**, *14*, 3156–3163. [CrossRef]
2. Rault, P.; Colas, F.; Guillaud, X.; Nguéfeu, S. Method for small signal stability analysis of VSC-MTDC grids. In Proceedings of the 2012 IEEE Power and Energy Society General Meeting, San Diego, CA, USA, 22–26 July 2012; pp. 1–7. [CrossRef]
3. Daniel, J.P.; Liu, S.; Ibanez, E.; Pennock, K.; Reed, G.; Hanes, S. *National Offshore Wind Energy Grid Interconnection Study*; ABB Inc.: Raleigh, NC, USA, 2014. [CrossRef]
4. Energy Sector Alliance Manitoba (ESAM). Atlantic Wind Connection Project. Available online: <http://energymanitoba.com/projects/atlantic-wind-connection-project/> (accessed on 30 October 2022).
5. Yazdani, A.; Iravani, R. *Voltage-Sourced Converters in Power Systems: Modeling, Control, and Applications*; John Wiley & Sons: New York, NY, USA, 2010.
6. Bahrman, M.P.; Johnson, B.K. The ABCs of HVDC transmission technologies. *IEEE Power Energy Mag.* **2007**, *5*, 32–44. [CrossRef]
7. Du, S.; Dekka, A.; Wu, B.; Zargari, N. *Modular Multilevel Converters: Analysis, Control, and Applications*; John Wiley & Sons: New York, NY, USA, 2018.
8. Sharifabadi, K.; Harnefors, L.; Nee, H.P.; Norrga, S.; Teodorescu, R. *Design, Control, and Application of Modular Multilevel Converters for HVDC Transmission Systems*; John Wiley & Sons: New York, NY, USA, 2016.
9. Nami, A.; Liang, J.; Dijkhuizen, F.; Demetriades, G.D. Modular Multilevel Converters for HVDC Applications: Review on Converter Cells and Functionalities. *IEEE Trans. Power Electron.* **2015**, *30*, 18–36. [CrossRef]
10. Sakib, M.N.; Azad, S.P.; Kazerani, M. A Critical Review of Modular Multilevel Converter Configurations and Submodule Topologies from DC Fault Blocking and Ride-Through Capabilities Viewpoints for HVDC Applications. *Energies* **2022**, *15*, 4176. [CrossRef]
11. Han, M.; Gole, A. *Modeling and Simulation of HVDC Transmission*; Institution of Engineering and Technology (IET): London, UK, 2020.
12. Pang, H.; Wei, X. Research on Key Technology and Equipment for Zhangbei 500kV DC Grid. In Proceedings of the 2018 International Power Electronics Conference (IPEC-Niigata 2018 ECCE Asia), Niigata, Japan, 20–24 May 2018; pp. 2343–2351. [CrossRef]
13. TenneT. NordLink. Available online: <https://www.tennet.eu/projects/nordlink> (accessed on 13 December 2022).
14. North Sea Link. Available online: <https://northsealink.com/> (accessed on 30 October 2022).
15. Chen, X.; Li, H.; Liang, Y.; Wang, G. A protection scheme for hybrid multi-terminal HVDC networks utilizing a time-domain transient voltage based on fault-blocking converters. *Int. J. Electr. Power Energy Syst.* **2020**, *118*, 105825. [CrossRef]
16. Hitachi Energy. Changji-Guquan UHVDC Link. Available online: <https://www.hitachienergy.com/case-studies/changji-guquan-uhvdc-link> (accessed on 30 October 2022).
17. ABB Commissions Historical Power Interconnector in Canada. Available online: <https://new.abb.com/news/detail/5053/abb-commissions-historical-power-interconnector-in-canada> (accessed on 30 October 2022).
18. Tang, G.; He, Z.; Pang, H.; Huang, X.; Zhang, X.p. Basic topology and key devices of the five-terminal DC grid. *CSEE J. Power Energy Syst.* **2015**, *1*, 22–35. [CrossRef]

19. Rao, H. Architecture of Nan'ao multi-terminal VSC-HVDC system and its multi-functional control. *CSEE J. Power Energy Syst.* **2015**, *1*, 9–18. [[CrossRef](#)]
20. Kong, M.; Pei, X.; Pang, H.; Yang, J.; Dong, X.; Wu, Y.; Zhou, X. A lifting wavelet-based protection strategy against DC line faults for Zhangbei HVDC Grid in China. In Proceedings of the 2017 19th European Conference on Power Electronics and Applications (EPE'17 ECCE Europe), Warsaw, Poland, 11–14 September 2017; pp. 1–11. [[CrossRef](#)]
21. Liu, J.; Tai, N.; Fan, C. Transient-Voltage-Based Protection Scheme for DC Line Faults in the Multiterminal VSC-HVDC System. *IEEE Trans. Power Deliv.* **2017**, *32*, 1483–1494. [[CrossRef](#)]
22. De Kerf, K.; Srivastava, K.; Reza, M.; Bekaert, D.; Cole, S.; Van Hertem, D.; Belmans, R. Wavelet-based protection strategy for DC faults in multi-terminal VSC HVDC systems. *IET Gener. Transm. Distrib.* **2011**, *5*, 496–503. [[CrossRef](#)]
23. Song, G.; Chu, X.; Gao, S.; Kang, X.; Jiao, Z. A New Whole-Line Quick-Action Protection Principle for HVDC Transmission Lines Using One-End Current. *IEEE Trans. Power Deliv.* **2015**, *30*, 599–607. [[CrossRef](#)]
24. Li, B.; He, J.; Li, Y.; Li, B. A review of the protection for the multi-terminal VSC-HVDC grid. *Prot. Control. Mod. Power Syst.* **2019**, *4*, 239–249. [[CrossRef](#)]
25. Zain Yousaf, M.; Liu, H.; Raza, A.; Baber Baig, M. Primary and backup fault detection techniques for multi-terminal HVdc systems: A review. *IET Gener. Transm. Distrib.* **2020**, *14*, 5261–5276. [[CrossRef](#)]
26. Perez-Molina, M.; Larruskain, D.; Eguia Lopez, P.; Buigues, G.; Valverde, V. Review of protection systems for multi-terminal high voltage direct current grids. *Renew. Sustain. Energy Rev.* **2021**, *144*, 111037. [[CrossRef](#)]
27. Recommendations to Improve HVDC Cable Systems Reliability—A Joint ENTSO-E and Europacable Paper. Available online: <https://www.entsoe.eu/2019/06/20/recommendations-to-improve-hvdc-cable-systems-reliability/> (accessed on 30 October 2022).
28. Jahn, I. Protection for Multiterminal HVDC Grids—A Digital Contribution. Ph.D. Thesis, KTH Royal Institute of Technology, Stockholm, Sweden, 2021.
29. Van Hertem, D.; Gomis-Bellmunt, O.; Liang, J. *HVDC Grids: For Offshore and Supergrid of the Future*; John Wiley & Sons: New York, NY, USA, 2016.
30. Jovicic, D. *High Voltage Direct Current Transmission: Converters, Systems and DC Grids*; John Wiley & Sons: New York, NY, USA, 2019.
31. Leterme, W. Communication-Less Protection Algorithms for Meshed VSC HVDC Cable Grids. Ph.D. Thesis, KU Leuven, Leuven, Belgium, 2016.
32. Belda, N.A.; Plet, C.A.; Smeets, R.P.P. Analysis of Faults in Multiterminal HVDC Grid for Definition of Test Requirements of HVDC Circuit Breakers. *IEEE Trans. Power Deliv.* **2018**, *33*, 403–411. [[CrossRef](#)]
33. Yang, J.; Fletcher, J.E.; O'Reilly, J. Multiterminal DC Wind Farm Collection Grid Internal Fault Analysis and Protection Design. *IEEE Trans. Power Deliv.* **2010**, *25*, 2308–2318. [[CrossRef](#)]
34. Leterme, W.; Ahmed, N.; Beerten, J.; Ångquist, L.; Hertem, D.V.; Norrga, S. A new HVDC grid test system for HVDC grid dynamics and protection studies in EMT-type software. In Proceedings of the 11th IET International Conference on AC and DC Power Transmission, Birmingham, UK, 10–12 February 2015. [[CrossRef](#)]
35. Li, C.; Zhao, C.; Xu, J.; Ji, Y.; Zhang, F.; An, T. A Pole-to-Pole Short-Circuit Fault Current Calculation Method for DC Grids. *IEEE Trans. Power Syst.* **2017**, *32*, 4943–4953. [[CrossRef](#)]
36. Wang, M.; Beerten, J.; Van Hertem, D. Frequency domain based DC fault analysis for bipolar HVDC grids. *J. Mod. Power Syst. Clean Energy* **2017**, *5*, 548–559. [[CrossRef](#)]
37. Leterme, W.; Tielens, P.; De Boeck, S.; Van Hertem, D. Overview of Grounding and Configuration Options for Meshed HVDC Grids. *IEEE Trans. Power Deliv.* **2014**, *29*, 2467–2475. [[CrossRef](#)]
38. Döring, D.; Würflinger, K.; Staudt, V.; Zeller, M.; Ebner, G. Interactions between a half-bridge MMC and a hybrid DC breaker during fault current interruption compared to a full-bridge MMC. *IET Power Electron.* **2020**, *13*, 4168–4175. [[CrossRef](#)]
39. Zhang, Y.; Cong, W.; Li, G.; Sun, K.; Zhang, Y. Single-ended MMC-MTDC line protection based on dual-frequency amplitude ratio of traveling wave. *Electr. Power Syst. Res.* **2020**, *189*, 106808. [[CrossRef](#)]
40. Leterme, W.; Van Hertem, D. Reduced Modular Multilevel Converter Model to Evaluate Fault Transients in DC Grids. In Proceedings of the 12th IET International Conference on Developments in Power System Protection (DPSP 2014), Copenhagen, Denmark, 31 March–3 April 2014.
41. Li, Y.; Li, J.; Wu, G.; Xiong, L.; Jia, K.; Xu, Z. DC Fault Analysis Models of Three Converter Topologies Considering Control Effects. *IEEE Trans. Ind. Electron.* **2020**, *67*, 9480–9491. [[CrossRef](#)]
42. Langwasser, M.; De Carne, G.; Liserre, M.; Biskoping, M. Fault Current Estimation in Multi-Terminal HVdc Grids Considering MMC Control. *IEEE Trans. Power Syst.* **2019**, *34*, 2179–2189. [[CrossRef](#)]
43. Gao, S.; Ye, H.; Liu, Y. Accurate and Efficient Estimation of Short-Circuit Current for MTDC Grids Considering MMC Control. *IEEE Trans. Power Deliv.* **2020**, *35*, 1541–1552. [[CrossRef](#)]
44. Luo, Y.; He, J.; Li, M.; Zhang, D.; Zhang, Y.; Song, Y.; Nie, M. Analytical Calculation of Transient Short-Circuit Currents for MMC-Based MTDC Grids. *IEEE Trans. Ind. Electron.* **2022**, *69*, 7500–7511. [[CrossRef](#)]
45. Guo, Y.; Li, H.; Liang, Y.; Wang, G. A Method to Calculate Short-Circuit Faults in High-Voltage DC Grids. *IEEE Trans. Power Deliv.* **2021**, *36*, 267–279. [[CrossRef](#)]
46. Ye, H.; Gao, S.; Li, G.; Liu, Y. Efficient Estimation and Characteristic Analysis of Short-Circuit Currents for MMC-MTDC Grids. *IEEE Trans. Ind. Electron.* **2021**, *68*, 258–269. [[CrossRef](#)]

47. Li, B.; Wang, W.; Li, B.; Liu, Y.; Wen, W.; Chen, X. Research on a current calculation method and characteristics of pole-to-ground faults in true bipolar MMC-HVDC grids considering line coupling. *Electr. Power Syst. Res.* **2021**, *192*, 106985. [[CrossRef](#)]
48. Tang, L.; Dong, X.; Shi, S.; Wang, B. Analysis of the characteristics of fault-induced travelling waves in MMC-HVDC grid. *J. Eng.* **2018**, *2018*, 1349–1353. [[CrossRef](#)]
49. Bucher, M.K.; Franck, C.M. Analytic Approximation of Fault Current Contributions From Capacitive Components in HVDC Cable Networks. *IEEE Trans. Power Deliv.* **2015**, *30*, 74–81. [[CrossRef](#)]
50. Bucher, M.K.; Franck, C.M. Contribution of Fault Current Sources in Multiterminal HVDC Cable Networks. *IEEE Trans. Power Deliv.* **2013**, *28*, 1796–1803. [[CrossRef](#)]
51. Wang, Y.; Yuan, Z.; Fu, J.; Li, Y.; Zhao, Y. A feasible coordination protection strategy for MMC-MTDC systems under DC faults. *Int. J. Electr. Power Energy Syst.* **2017**, *90*, 103–111. [[CrossRef](#)]
52. CIGRE Joint Working Group B4/B5.59. TB 739: Protection and Local Control of HVDC-Grids. 2018. Available online: <https://e-cigre.org/publication/739-protection-and-local-control-of-hvdc-grids> (accessed on 30 October 2022).
53. Ruffing, P.; Collath, N.; Brantl, C.; Schnettler, A. DC Fault Control and High-Speed Switch Design for an HVDC Network Protection Based on Fault-Blocking Converters. *IEEE Trans. Power Deliv.* **2019**, *34*, 397–406. [[CrossRef](#)]
54. Mohammadi, F.; Rouzbehi, K.; Hajian, M.; Niayesh, K.; Gharehpetian, G.B.; Saad, H.; Hasan Ali, M.; Sood, V.K. HVDC Circuit Breakers: A Comprehensive Review. *IEEE Trans. Power Electron.* **2021**, *36*, 13726–13739. [[CrossRef](#)]
55. Smeets, R.P.P.; Belda, N.A. High-voltage direct current fault current interruption: A technology review. *High Volt.* **2021**, *6*, 171–192. [[CrossRef](#)]
56. Tahata, K.; Oukaili, S.E.; Kamei, K.; Yoshida, D.; Kono, Y.; Yamamoto, R.; Ito, H. HVDC circuit breakers for HVDC grid applications. In Proceedings of the 11th IET International Conference on AC and DC Power Transmission, Birmingham, UK, 10–12 February 2015. [[CrossRef](#)]
57. Lin, W.; Jovicic, D.; Nguéfeu, S.; Saad, H. Modelling of high-power hybrid DC circuit breaker for grid-level studies. *IET Power Electron.* **2016**, *9*, 237–246. [[CrossRef](#)]
58. Yang, Y.; Ren, M.; Cao, J.; Liu, W.; Zhan, X.; Zhao, C. HVDC Circuit Breaker Development and Applications in VSC-HVDC Transmission Project. *IOP Conf. Ser. Earth Environ. Sci.* **2020**, *453*, 012048. [[CrossRef](#)]
59. Chen, W.; Zeng, R.; He, J.; Wu, Y.; Wei, X.; Fang, T.; et al. Development and prospect of direct-current circuit breaker in China. *High Volt.* **2021**, *6*, 1–15. [[CrossRef](#)]
60. Jahn, I.; Johannesson, N.; Norrga, S. Survey of Methods for Selective DC Fault Detection in MTDC Grids. In Proceedings of the 13th IET International Conference on AC and DC Power Transmission (ACDC 2017), Manchester, UK, 14–16 February 2017.
61. Leterme, W.; Jahn, I.; Ruffing, P.; Sharifabadi, K.; Van Hertem, D. Designing for High-Voltage dc Grid Protection: Fault Clearing Strategies and Protection Algorithms. *IEEE Power Energy Mag.* **2019**, *17*, 73–81. [[CrossRef](#)]
62. Jahn, I.; Nahalparvari, M.; Hirsching, C.; Hoffmann, M.; Düllmann, P.; Loku, F.; Agbemuko, A.; Chaffey, G.; Prieto-Araujo, E.; Norrga, S. An Architecture for a Multi-Vendor VSC-HVDC Station With Partially Open Control and Protection. *IEEE Access* **2022**, *10*, 13555–13569. [[CrossRef](#)]
63. Wang, M.; Leterme, W.; Chaffey, G.; Beerten, J.; Van Hertem, D. Multi-vendor interoperability in HVDC grid protection: State-of-the-art and challenges ahead. *IET Gener. Transm. Distrib.* **2021**, *15*, 2153–2175. [[CrossRef](#)]
64. Third ENTSO-E Position Paper on Offshore Development Focuses on Interoperability. Available online: <https://preview.entsoe.eu/news/2021/01/25/third-entso-e-position-paper-on-offshore-development-focuses-on-interoperability/> (accessed on 30 October 2022).
65. BEST PATHS. D9.3: BEST PATHS DEMO2: Final Recommendations For Interoperability Of Multivendor HVDC Systems. Available online: <http://www.bestpaths-project.eu/contents/publications/d93--final-demo2-recommendations--vfinal.pdf> (accessed on 30 October 2022).
66. Li, Z.; Ye, Y.; Tong, N.; Lin, X.; Li, C.; Jin, N.; Chen, L. High error-tolerable unit protection for VSC-MTDC independent of data synchronization. *Int. J. Electr. Power Energy Syst.* **2021**, *124*, 106393. [[CrossRef](#)]
67. Ma, J.; Xiao, Z.; Li, Y.; Zhang, J.; Wu, B.; Li, Z.; Ma, R.; Huang, W.; Cheng, P. A new pilot protection scheme for modular multi-level converter-based HVDC system based on voltage matching factor. *IET Gener. Transm. Distrib.* **2022**, *16*, 2573–2586. [[CrossRef](#)]
68. Nadeem, M.H.; Zheng, X.; Tai, N.; Gul, M.; Yu, M.; He, Y. Non-communication based protection scheme using transient harmonics for multi-terminal HVDC networks. *Int. J. Electr. Power Energy Syst.* **2021**, *127*, 106636. [[CrossRef](#)]
69. Tong, N.; Lin, X.; Li, Y.; Hu, Z.; Jin, N.; Wei, F.; Li, Z. Local Measurement-Based Ultra-High-Speed Main Protection for Long Distance VSC-MTDC. *IEEE Trans. Power Deliv.* **2019**, *34*, 353–364. [[CrossRef](#)]
70. Haleem, N.M.; Rajapakse, A.D. Application of new directional logic to improve DC side fault discrimination for high resistance faults in HVDC grids. *J. Mod. Power Syst. Clean Energy* **2017**, *5*, 560–573. [[CrossRef](#)]
71. Haleem, N.M.; Rajapakse, A.D. Local measurement based ultra-fast directional ROCOV scheme for protecting Bi-pole HVDC grids with a metallic return conductor. *Int. J. Electr. Power Energy Syst.* **2018**, *98*, 323–330. [[CrossRef](#)]
72. Li, S.; Chen, W.; Yin, X.; Chen, D.; Teng, Y. A Novel Integrated Protection for VSC-HVDC Transmission Line Based on Current Limiting Reactor Power. *IEEE Trans. Power Deliv.* **2020**, *35*, 226–233. [[CrossRef](#)]
73. Li, C.; Gole, A.M.; Zhao, C. A Fast DC Fault Detection Method Using DC Reactor Voltages in HVdc Grids. *IEEE Trans. Power Deliv.* **2018**, *33*, 2254–2264. [[CrossRef](#)]

74. Pirooz Azad, S.; Leterme, W.; Van Hertem, D. Fast breaker failure backup protection for HVDC grids. *Electr. Power Syst. Res.* **2016**, *138*, 99–105. [[CrossRef](#)]
75. Leterme, W.; Pirooz Azad, S.; Van Hertem, D. A Local Backup Protection Algorithm for HVDC Grids. *IEEE Trans. Power Deliv.* **2016**, *31*, 1767–1775. [[CrossRef](#)]
76. Luo, S.; Dong, X.; Shi, S.; Wang, B. A Directional Protection Scheme for HVDC Transmission Lines Based on Reactive Energy. *IEEE Trans. Power Deliv.* **2016**, *31*, 559–567. [[CrossRef](#)]
77. Zhang, Y.; Li, Y.; Song, J.; Li, B.; Chen, X. A New Protection Scheme for HVDC Transmission Lines Based on the Specific Frequency Current of DC Filter. *IEEE Trans. Power Deliv.* **2019**, *34*, 420–429. [[CrossRef](#)]
78. Huai, Q.; Liu, K.; Qin, L.; Liao, X.; Zhu, S.; Li, Y.; Ding, H. Backup-Protection Scheme for Multi-Terminal HVDC System Based on Wavelet-Packet-Energy Entropy. *IEEE Access* **2019**, *7*, 49790–49803. [[CrossRef](#)]
79. Tong, N.; Lin, X.; Li, C.; Sui, Q.; Chen, L.; Wang, Z.; Jin, N.; Li, Z. Permissive pilot protection adaptive to DC fault interruption for VSC-MTDC. *Int. J. Electr. Power Energy Syst.* **2020**, *123*, 106234. [[CrossRef](#)]
80. Yu, S.; Wang, X.; Pang, C. A Pilot Protection Scheme of DC Lines for MMC-HVDC Grid using Random Matrix. *J. Mod. Power Syst. Clean Energy* **2022**, 1–17. [[CrossRef](#)]
81. Abu-Elanien, A.E.; Elserougi, A.A.; Abdel-Khalik, A.S.; Massoud, A.M.; Ahmed, S. A differential protection technique for multi-terminal HVDC. *Electr. Power Syst. Res.* **2016**, *130*, 78–88. [[CrossRef](#)]
82. Hajian, M.; Zhang, L.; Jovcic, D. DC Transmission Grid With Low-Speed Protection Using Mechanical DC Circuit Breakers. *IEEE Trans. Power Deliv.* **2015**, *30*, 1383–1391. [[CrossRef](#)]
83. Jovcic, D.; Lin, W.; Nguéfeu, S.; Saad, H. Low-Energy Protection System for DC Grids Based on Full-Bridge MMC Converters. *IEEE Trans. Power Deliv.* **2018**, *33*, 1934–1943. [[CrossRef](#)]
84. Liu, H.; Li, B.; Wen, W.; Green, T.C.; Zhang, J.; Zhang, N.; Chen, L. Ultra-fast current differential protection with high-sensitivity for HVDC transmission lines. *Int. J. Electr. Power Energy Syst.* **2021**, *126*, 106580. [[CrossRef](#)]
85. Gao, S.p.; Liu, Q.; Song, G.b. Current differential protection principle of HVDC transmission system. *IET Gener. Transm. Distrib.* **2017**, *11*, 1286–1292. [[CrossRef](#)]
86. Xue, S.; Lu, J.; Sun, Y.; Wang, S.; Li, B.; Li, B. A reverse travelling wave differential protection scheme for DC lines in MMC-HVDC system with metallic return. *Int. J. Electr. Power Energy Syst.* **2022**, *135*, 107521. [[CrossRef](#)]
87. Li, B.; Lv, M.; Li, B.; Xue, S.; Wen, W. Research on an Improved Protection Principle Based on Differential Voltage Traveling Wave for VSC-HVDC Transmission Lines. *IEEE Trans. Power Deliv.* **2020**, *35*, 2319–2328. [[CrossRef](#)]
88. Song, G.; Chu, X.; Cai, X.; Gao, S. A novel pilot protection principle for VSC-HVDC cable lines based on fault component current. *Int. J. Electr. Power Energy Syst.* **2013**, *53*, 426–433. [[CrossRef](#)]
89. Zou, G.; Feng, Q.; Huang, Q.; Sun, C.; Gao, H. A fast protection scheme for VSC based multi-terminal DC grid. *Int. J. Electr. Power Energy Syst.* **2018**, *98*, 307–314. [[CrossRef](#)]
90. Huang, Q.; Zou, G.; Zhang, S.; Gao, H. A Pilot Protection Scheme of DC Lines for Multi-Terminal HVDC Grid. *IEEE Trans. Power Deliv.* **2019**, *34*, 1957–1966. [[CrossRef](#)]
91. He, J.; Li, B.; Li, Y.; Qiu, H.; Wang, C.; Dai, D. A Fast Directional Pilot Protection Scheme for the MMC-based MTDC Grid. *Proc. Chin. Soc. Electr. Eng.* **2017**, *37*, 6878–6887. [[CrossRef](#)]
92. Xiang, W.; Yang, S.; Adam, G.P.; Zhang, H.; Zuo, W.; Wen, J. DC Fault Protection Algorithms of MMC-HVDC Grids: Fault Analysis, Methodologies, Experimental Validations, and Future Trends. *IEEE Trans. Power Electron.* **2021**, *36*, 11245–11264. [[CrossRef](#)]
93. Leterme, W.; Van Hertem, D. Cable Protection in HVDC Grids Employing Distributed Sensors and Proactive HVDC Breakers. *IEEE Trans. Power Deliv.* **2018**, *33*, 1981–1990. [[CrossRef](#)]
94. Li, Y.; Gong, Y.; Jiang, B. A novel traveling-wave-based directional protection scheme for MTDC grid with inductive DC terminal. *Electr. Power Syst. Res.* **2018**, *157*, 83–92. [[CrossRef](#)]
95. Wang, D.; Yu, D.; Yang, H.; Hou, M.; Guo, Y. Novel travelling wave directional pilot protection for VSC-HVDC transmission line. *IET Gener. Transm. Distrib.* **2020**, *14*, 1705–1713. [[CrossRef](#)]
96. Zheng, X.; Nadeem, M.H.; Tai, N.; Habib, S.; Wang, B.; Yu, M.; He, Y. A transient current protection and fault location scheme for MMC-HVDC transmission network. *Int. J. Electr. Power Energy Syst.* **2021**, *124*, 106348. [[CrossRef](#)]
97. Zhao, P.; Chen, Q.; Sun, K. A novel protection method for VSC-MTDC cable based on the transient DC current using the S transform. *Int. J. Electr. Power Energy Syst.* **2018**, *97*, 299–308. [[CrossRef](#)]
98. Jiang, L.; Chen, Q.; Huang, W.; Wang, L.; Zeng, Y.; Zhao, P. Pilot Protection Based on Amplitude of Directional Travelling Wave for Voltage Source Converter-High Voltage Direct Current (VSC-HVDC) Transmission Lines. *Energies* **2018**, *11*, 2021. [[CrossRef](#)]
99. Zheng, X.; Tai, N.; Wu, Z.; Thorp, J. Harmonic current protection scheme for voltage source converter-based high-voltage direct current transmission system. *IET Gener. Transm. Distrib.* **2014**, *8*, 1509–1515. [[CrossRef](#)]
100. Ashouri, M.; Faria da Silva, F.; Leth Bak, C. A Harmonic Based Pilot Protection Scheme for VSC-MTDC Grids with PWM Converters. *Energies* **2019**, *12*, 1010. [[CrossRef](#)]
101. Xiang, W.; Zhang, H.; Yang, S.; Zhou, M.; Lin, W.; Wen, J. A Differential Pilot Protection Scheme for MMC-Based DC Grid Resilient to Communication Failure. *IEEE J. Emerg. Sel. Top. Power Electron.* **2021**, *9*, 5631–5645. [[CrossRef](#)]
102. Farshad, M. A Pilot Protection Scheme for Transmission Lines of Half-Bridge MMC-HVDC Grids Using Cosine Distance Criterion. *IEEE Trans. Power Deliv.* **2021**, *36*, 1089–1096. [[CrossRef](#)]

103. Huai, Q.; Qin, L.; Liu, K.; Hooshyar, A.; Ding, H.; Gong, C.; Xu, Y. A pilot line protection for MT-HVDC grids using similarity of traveling waveforms. *Int. J. Electr. Power Energy Syst.* **2021**, *131*, 107162. [[CrossRef](#)]
104. He, J.; Li, B.; Li, Y.; Wang, W.; Lyu, H.; Li, B. Simplified calculation method of threshold value for the non-unit transient-voltage based protection in multi-terminal VSC-HVDC grid. *Int. J. Electr. Power Energy Syst.* **2022**, *134*, 107435. [[CrossRef](#)]
105. Sneath, J.; Rajapakse, A.D. Fault Detection and Interruption in an Earthed HVDC Grid Using ROCOV and Hybrid DC Breakers. *IEEE Trans. Power Deliv.* **2016**, *31*, 973–981. [[CrossRef](#)]
106. Sneath, J.; Rajapakse, A.D. DC Fault Protection of a Nine-Terminal MMC HVDC Grid. In Proceedings of the 11th IET International Conference on AC and DC Power Transmission, Birmingham, UK, 10–12 February 2015. [[CrossRef](#)]
107. Leterme, W.; Beerten, J.; Van Hertem, D. Nonunit Protection of HVDC Grids With Inductive DC Cable Termination. *IEEE Trans. Power Deliv.* **2016**, *31*, 820–828. [[CrossRef](#)]
108. Haleem, N.M.; Rajapakse, A.D. Fault-Type Discrimination in HVDC Transmission Lines Using Rate of Change of Local Currents. *IEEE Trans. Power Deliv.* **2020**, *35*, 117–129. [[CrossRef](#)]
109. Raza, A.; Akhtar, A.; Jamil, M.; Abbas, G.; Gilani, S.O.; Yuchao, L.; Khan, M.N.; Izhar, T.; Dianguo, X.; Williams, B.W. A Protection Scheme for Multi-Terminal VSC-HVDC Transmission Systems. *IEEE Access* **2018**, *6*, 3159–3166. [[CrossRef](#)]
110. Yang, J.; Fletcher, J.; O'Reilly, J.; Adam, G.; Fan, S. Protection scheme design for meshed VSC-HVDC transmission systems of large-scale wind farms. In Proceedings of the 9th IET International Conference on AC and DC Power Transmission (ACDC 2010), London, UK, 19–21 October 2010. [[CrossRef](#)]
111. Stumpe, M.; Tünnerhoff, P.; Dave, J.; Schnettler, A.; Ergin, D.; Schön, A.; Würflinger, K.; Schettler, F. DC fault protection for modular multi-level converter-based HVDC multi-terminal systems with solid state circuit breakers. *IET Gener. Transm. Distrib.* **2018**, *12*, 3013–3020. [[CrossRef](#)]
112. Pirooz Azad, S.; Van Hertem, D. A Fast Local Bus Current-Based Primary Relaying Algorithm for HVDC Grids. *IEEE Trans. Power Deliv.* **2017**, *32*, 193–202. [[CrossRef](#)]
113. Pirooz Azad, S.; Leterme, W.; Van Hertem, D. A DC grid primary protection algorithm based on current measurements. In Proceedings of the 2015 17th European Conference on Power Electronics and Applications (EPE'15 ECCE-Europe), Geneva, Switzerland, 8–10 September 2015. [[CrossRef](#)]
114. Tzelepis, D.; Dyško, A.; Fusiek, G.; Nelson, J.; Niewczas, P.; Vozikis, D.; Orr, P.; Gordon, N.; Booth, C.D. Single-Ended Differential Protection in MTDC Networks Using Optical Sensors. *IEEE Trans. Power Deliv.* **2017**, *32*, 1605–1615. [[CrossRef](#)]
115. Li, S.; Chen, W.; Yin, X.; Chen, D. Protection scheme for VSC-HVDC transmission lines based on transverse differential current. *IET Gener. Transm. Distrib.* **2017**, *11*, 2805–2813. [[CrossRef](#)]
116. Ashrafi Niaki, S.H.; Hosseini, S.M.; Abdoos, A.A. Fault detection of HVDC cable in multi-terminal offshore wind farms using transient sheath voltage. *IET Renew. Power Gener.* **2017**, *11*, 1707–1713. [[CrossRef](#)]
117. Elgeziry, M.; Elsadd, M.; Elkalashy, N.; Kawady, T.; Taalab, A.M.; Izzularab, M.A. Non-pilot protection scheme for multi-terminal VSC-HVDC transmission systems. *IET Renew. Power Gener.* **2019**, *13*, 3033–3042. [[CrossRef](#)]
118. Huang, Q.; Zou, G.; Wei, X.; Sun, C.; Gao, H. A non-unit line protection scheme for MMC-based multi-terminal HVDC grid. *Int. J. Electr. Power Energy Syst.* **2019**, *107*, 1–9. [[CrossRef](#)]
119. Mehrabi-Kooshki, M.; Mirhosseini, S.S.; Jamali, S. Non-unit protection scheme for HVDC transmission lines based on energy of voltage difference. *IET Gener. Transm. Distrib.* **2022**, *16*, 2166–2187. [[CrossRef](#)]
120. Liao, J.; Zhou, N.; Wang, Q. DC Grid Protection Method Based on Phase Planes of Single-End Common-and Differential-Mode Components. *IEEE Trans. Power Deliv.* **2021**, *36*, 299–310. [[CrossRef](#)]
121. Troitzsch, C.; Marten, A.K.; Westermann, D. Non-telecommunication based DC line fault detection methodology for meshed HVDC grids. *IET Gener. Transm. Distrib.* **2016**, *10*, 4231–4239. [[CrossRef](#)]
122. Li, Y.; Wu, L.; Li, J.; Xiong, L.; Zhang, X.; Song, G.; Xu, Z. DC Fault Detection in MTDC Systems Based on Transient High Frequency of Current. *IEEE Trans. Power Deliv.* **2019**, *34*, 950–962. [[CrossRef](#)]
123. Li, Y.; Li, J.; Xiong, L.; Zhang, X.; Xu, Z. DC Fault Detection in Meshed MTdc Systems Based on Transient Average Value of Current. *IEEE Trans. Ind. Electron.* **2020**, *67*, 1932–1943. [[CrossRef](#)]
124. Li, R.; Xu, L.; Yao, L. DC Fault Detection and Location in Meshed Multiterminal HVDC Systems Based on DC Reactor Voltage Change Rate. *IEEE Trans. Power Deliv.* **2017**, *32*, 1516–1526. [[CrossRef](#)]
125. He, Y.; Zheng, X.; Tai, N.; Wang, J.; Nadeem, M.H.; Liu, J. A DC Line Protection Scheme for MMC-Based DC Grids Based on AC/DC Transient Information. *IEEE Trans. Power Deliv.* **2020**, *35*, 2800–2811. [[CrossRef](#)]
126. Dadgostar, H.; Hajian, M.; Ahmed, K. DC grids DC fault detection using asymmetric pole inductors. *Electr. Power Syst. Res.* **2021**, *193*, 107016. [[CrossRef](#)]
127. Tzelepis, D.; Dyško, A.; Blair, S.M.; Rousis, A.O.; Mirsaiedi, S.; Booth, C.; Dong, X. Centralised busbar differential and wavelet-based line protection system for multi-terminal direct current grids, with practical IEC-61869-compliant measurements. *IET Gener. Transm. Distrib.* **2018**, *12*, 3578–3586. [[CrossRef](#)]
128. Abu-Elanien, A.E.; Abdel-Khalik, A.S.; Massoud, A.M.; Ahmed, S. A non-communication based protection algorithm for multi-terminal HVDC grids. *Electr. Power Syst. Res.* **2017**, *144*, 41–51. [[CrossRef](#)]
129. Xiang, W.; Yang, S.; Xu, L.; Zhang, J.; Lin, W.; Wen, J. A Transient Voltage-Based DC Fault Line Protection Scheme for MMC-Based DC Grid Embedding DC Breakers. *IEEE Trans. Power Deliv.* **2019**, *34*, 334–345. [[CrossRef](#)]

130. Mitra, B.; Chowdhury, B.; Willis, A. Protection Coordination for Assembly HVDC Breakers for HVDC Multiterminal Grids Using Wavelet Transform. *IEEE Syst. J.* **2020**, *14*, 1069–1079. [[CrossRef](#)]
131. Li, B.; Li, Y.; He, J.; Li, B.; Liu, S.; Liu, B.; Xu, L. An Improved Transient Traveling-Wave Based Direction Criterion for Multi-Terminal HVDC Grid. *IEEE Trans. Power Deliv.* **2020**, *35*, 2517–2529. [[CrossRef](#)]
132. He, Z.y.; Liao, K. Natural frequency-based protection scheme for voltage source converter-based high-voltage direct current transmission lines. *IET Gener. Transm. Distrib.* **2015**, *9*, 1519–1525. [[CrossRef](#)]
133. Duan, J.; Li, H.; Lei, Y.; Tuo, L. A novel non-unit transient based boundary protection for HVDC transmission lines using synchrosqueezing wavelet transform. *Int. J. Electr. Power Energy Syst.* **2020**, *115*, 105478. [[CrossRef](#)]
134. Yeap, Y.M.; Geddada, N.; Satpathi, K.; Ukil, A. Time- and Frequency-Domain Fault Detection in a VSC-Interfaced Experimental DC Test System. *IEEE Trans. Ind. Inform.* **2018**, *14*, 4353–4364. [[CrossRef](#)]
135. Li, J.; Yang, Q.; Mu, H.; Le Blond, S.; He, H. A new fault detection and fault location method for multi-terminal high voltage direct current of offshore wind farm. *Appl. Energy* **2018**, *220*, 13–20. [[CrossRef](#)]
136. Saleh, K.A.; Hooshyar, A.; El-Saadany, E.F.; Zeineldin, H.H. Protection of High-Voltage DC Grids Using Traveling-Wave Frequency Characteristics. *IEEE Syst. J.* **2020**, *14*, 4284–4295. [[CrossRef](#)]
137. Huang, N.E.; Wu, Z. A review on Hilbert-Huang transform: Method and its applications to geophysical studies. *Rev. Geophys.* **2008**, *46*, RG2006. [[CrossRef](#)]
138. Albernaz Lacerda, V.; Monaro, R.M.; Campos-Gaona, D.; Coury, D.V.; Anaya-Lara, O. Distance protection algorithm for multiterminal HVDC systems using the Hilbert–Huang transform. *IET Gener. Transm. Distrib.* **2020**, *14*, 3022–3032. [[CrossRef](#)]
139. Li, D.; Ukil, A.; Satpathi, K.; Yeap, Y.M. Hilbert–Huang Transform Based Transient Analysis in Voltage Source Converter Interfaced Direct Current System. *IEEE Trans. Ind. Electron.* **2021**, *68*, 11014–11025. [[CrossRef](#)]
140. Zhang, Y.; Tai, N.; Xu, B. Fault Analysis and Traveling-Wave Protection Scheme for Bipolar HVDC Lines. *IEEE Trans. Power Deliv.* **2012**, *27*, 1583–1591. [[CrossRef](#)]
141. Yang, S.; Xiang, W.; Li, R.; Lu, X.; Zuo, W.; Wen, J. An Improved DC Fault Protection Algorithm for MMC HVDC Grids Based on Modal-Domain Analysis. *IEEE J. Emerg. Sel. Top. Power Electron.* **2020**, *8*, 4086–4099. [[CrossRef](#)]
142. Yu, X.; Xiao, L. A DC Fault Protection Scheme for MMC-HVDC Grids Using New Directional Criterion. *IEEE Trans. Power Deliv.* **2021**, *36*, 441–451. [[CrossRef](#)]
143. Verrax, P.; Bertinato, A.; Kieffer, M.; Raison, B. Transient-based fault identification algorithm using parametric models for meshed HVDC grids. *Electr. Power Syst. Res.* **2020**, *185*, 106387. [[CrossRef](#)]
144. Suonan, J.; Zhang, J.; Jiao, Z.; Yang, L.; Song, G. Distance Protection for HVDC Transmission Lines Considering Frequency-Dependent Parameters. *IEEE Trans. Power Deliv.* **2013**, *28*, 723–732. [[CrossRef](#)]
145. Qin, Y.; Wen, M.; Zheng, J.; Bai, Y. A novel distance protection scheme for HVDC lines based on R-L model. *Int. J. Electr. Power Energy Syst.* **2018**, *100*, 167–177. [[CrossRef](#)]
146. Zheng, J.; Li, P.; Xu, K.; Kong, X.; Wang, C.; Lin, J.; Zhang, C. A distance protection scheme for HVDC transmission lines based on the Steady-state parameter model. *Int. J. Electr. Power Energy Syst.* **2022**, *136*, 107658. [[CrossRef](#)]
147. Lacerda, V.A.; Monaro, R.M.; Peña-Alzola, R.; Campos-Gaona, D.; Coury, D.V. Nonunit Distance Protection Algorithm for Multiterminal MMC-HVdc Systems Using DC Capacitor Resonance Frequency. *IEEE Trans. Ind. Electron.* **2022**, *69*, 12924–12933. [[CrossRef](#)]
148. Qin, Y.; Wen, M.; Yin, X.; Bai, Y.; Fang, Z. A novel distance protection for MMC-HVDC lines based on the equivalent capacitance voltage. *Int. J. Electr. Power Energy Syst.* **2022**, *137*, 107850. [[CrossRef](#)]
149. Yang, Q.; Le Blond, S.; Aggarwal, R.; Wang, Y.; Li, J. New ANN method for multi-terminal HVDC protection relaying. *Electr. Power Syst. Res.* **2017**, *148*, 192–201. [[CrossRef](#)]
150. Abu-Elanien, A.E.B. An Artificial Neural Network Based Technique for Protection of HVDC Grids. In Proceedings of the 2019 IEEE PES GTD Grand International Conference and Exposition Asia (GTD Asia), Bangkok, Thailand, 20–23 March 2019; pp. 1004–1009. [[CrossRef](#)]
151. Bertho, R.; Lacerda, V.A.; Monaro, R.M.; Vieira, J.C.M.; Coury, D.V. Selective Nonunit Protection Technique for Multiterminal VSC-HVDC Grids. *IEEE Trans. Power Deliv.* **2018**, *33*, 2106–2114. [[CrossRef](#)]
152. Tong, N.; Tang, Z.; Wang, Y.; Lai, C.S.; Lai, L.L. Semi AI-based protection element for MMC-MTDC using local-measurements. *Int. J. Electr. Power Energy Syst.* **2022**, *142*, 108310. [[CrossRef](#)]
153. Jamali, S.; Mirhosseini, S.S. Protection of transmission lines in multi-terminal HVDC grids using travelling waves morphological gradient. *Int. J. Electr. Power Energy Syst.* **2019**, *108*, 125–134. [[CrossRef](#)]
154. Mirhosseini, S.S.; Jamali, S.; Popov, M. Non-unit protection method for long transmission lines in MTDC grids. *IET Gener. Transm. Distrib.* **2021**, *15*, 1674–1687. [[CrossRef](#)]
155. Liu, L.; Liu, Z.; Popov, M.; Palensky, P.; van der Meijden, M.A.M.M. A Fast Protection of Multi-Terminal HVDC System Based on Transient Signal Detection. *IEEE Trans. Power Deliv.* **2021**, *36*, 43–51. [[CrossRef](#)]
156. Zhang, C.; Song, G.; Dong, X. A Novel Traveling Wave Protection Method for DC Transmission Lines Using Current Fitting. *IEEE Trans. Power Deliv.* **2020**, *35*, 2980–2991. [[CrossRef](#)]
157. Zhang, C.; Song, G.; Wang, T.; Wu, L.; Yang, L. Non-unit Traveling Wave Protection of HVDC Grids Using Levenberg–Marquart Optimal Approximation. *IEEE Trans. Power Deliv.* **2020**, *35*, 2260–2271. [[CrossRef](#)]

158. Zhang, C.; Song, G.; Wang, T.; Dong, X. An Improved Non-Unit Traveling Wave Protection Method With Adaptive Threshold Value and Its Application in HVDC Grids. *IEEE Trans. Power Deliv.* **2020**, *35*, 1800–1811. [[CrossRef](#)]
159. Shu, H.; Wang, G.; Tian, X.; Lei, S.; Jiang, X.; Bo, Z. Single-ended protection method of MMC-HVDC transmission line based on random matrix theory. *Int. J. Electr. Power Energy Syst.* **2022**, *142*, 108299. [[CrossRef](#)]
160. Farshad, M. Ultra-high-speed non-unit non-differential protection scheme for buses of MMC-HVDC grids. *IET Renew. Power Gener.* **2020**, *14*, 1541–1549. [[CrossRef](#)]
161. Nanayakkara, O.M.K.K.; Rajapakse, A.D.; Wachal, R. Location of DC Line Faults in Conventional HVDC Systems With Segments of Cables and Overhead Lines Using Terminal Measurements. *IEEE Trans. Power Deliv.* **2012**, *27*, 279–288. [[CrossRef](#)]
162. Nanayakkara, O.M.K.K.; Rajapakse, A.D.; Wachal, R. Traveling-Wave-Based Line Fault Location in Star-Connected Multiterminal HVDC Systems. *IEEE Trans. Power Deliv.* **2012**, *27*, 2286–2294. [[CrossRef](#)]
163. Panahi, H.; Sanaye-Pasand, M.; Zamani, R.; Mehrjerdi, H. A Novel DC Transmission System Fault Location Technique for Offshore Renewable Energy Harvesting. *IEEE Trans. Power Deliv.* **2020**, *35*, 2885–2895. [[CrossRef](#)]
164. Mahfouz, M.M.; El-Sayed, M.A. One-end protection algorithm for offshore wind farm HVDC transmission based on travelling waves and cross-alienation. *Electr. Power Syst. Res.* **2020**, *185*, 106355. [[CrossRef](#)]
165. Huai, Q.; Liu, K.; Hooshyar, A.; Ding, H.; Qin, L.; Chen, K. Line fault location for multi-terminal MMC-HVDC system based on SWT and SVD. *IET Renew. Power Gener.* **2020**, *14*, 4043–4052. [[CrossRef](#)]
166. Yang, J.; Fletcher, J.E.; O'Reilly, J. Short-Circuit and Ground Fault Analyses and Location in VSC-Based DC Network Cables. *IEEE Trans. Ind. Electron.* **2012**, *59*, 3827–3837. [[CrossRef](#)]
167. Farshad, M.; Sadeh, J. A Novel Fault-Location Method for HVDC Transmission Lines Based on Similarity Measure of Voltage Signals. *IEEE Trans. Power Deliv.* **2013**, *28*, 2483–2490. [[CrossRef](#)]
168. Azizi, S.; Sanaye-Pasand, M.; Abedini, M.; Hasani, A. A Traveling-Wave-Based Methodology for Wide-Area Fault Location in Multiterminal DC Systems. *IEEE Trans. Power Deliv.* **2014**, *29*, 2552–2560. [[CrossRef](#)]
169. Huai, Q.; Liu, K.; Hooshyar, A.; Ding, H.; Chen, K.; Liang, Q. Single-ended line fault location method for multi-terminal HVDC system based on optimized variational mode decomposition. *Electr. Power Syst. Res.* **2021**, *194*, 107054. [[CrossRef](#)]
170. Wang, J.; Zhang, Y.; Li, T. Equivalent characteristic impedance based hybrid-HVDC transmission line fault location. *Electr. Power Syst. Res.* **2021**, *194*, 107055. [[CrossRef](#)]
171. Lacerda, V.A.; Monaro, R.M.; Coury, D.V. Fault distance estimation in multiterminal HVDC systems using the Lomb-Scargle periodogram. *Electr. Power Syst. Res.* **2021**, *196*, 107251. [[CrossRef](#)]
172. Dardengo, V.P.; Fardin, J.F.; de Almeida, M.C. Single-terminal fault location in HVDC lines with accurate wave velocity estimation. *Electr. Power Syst. Res.* **2021**, *194*, 107057. [[CrossRef](#)]
173. Xiaoguang, Z.; Chunying, H.; Junbo, D.; Yubo, G.; Xiaohui, C. Research on a Highly Precise Fault Location Method for ± 1100 kV UHVDC Transmission Lines Based on Hilbert-Huang Transform. In Proceedings of the 2019 IEEE 8th International Conference on Advanced Power System Automation and Protection (APAP), Xi'an, China, 21–24 October 2019; pp. 850–854. [[CrossRef](#)]
174. Wang, D.; Hou, M. Travelling wave fault location algorithm for LCC-MMC-MTDC hybrid transmission system based on Hilbert-Huang transform. *Int. J. Electr. Power Energy Syst.* **2020**, *121*, 106125. [[CrossRef](#)]
175. Mehdi, A.; Kim, C.H.; Hussain, A.; Kim, J.S.; Hassan, S.J.U. A Comprehensive Review of Auto-Reclosing Schemes in AC, DC, and Hybrid (AC/DC) Transmission Lines. *IEEE Access* **2021**, *9*, 74325–74342. [[CrossRef](#)]
176. Wen, W.; Liu, H.; Li, B.; Li, P.; Zhang, N.; Gao, C.; Wang, C. Novel Reclosing Strategy Based on Transient Operating Voltage in Pseudobipolar DC System With Mechanical DCCB. *IEEE Trans. Power Electron.* **2021**, *36*, 4125–4133. [[CrossRef](#)]
177. Li, B.; Mao, Q.; He, J.; Li, Y.; Wu, T.; Dai, W.; Li, X.; Yu, Q. Adaptive reclosing strategy for the mechanical DC circuit breaker in VSC-HVDC grid. *Electr. Power Syst. Res.* **2021**, *192*, 107008. [[CrossRef](#)]
178. Li, B.; He, J.; Li, Y.; Wen, W. A Novel DCCB Reclosing Strategy for the Flexible HVDC Grid. *IEEE Trans. Power Deliv.* **2020**, *35*, 244–257. [[CrossRef](#)]
179. Yang, S.; Xiang, W.; Lu, X.; Zuo, W.; Wen, J. An Adaptive Reclosing Strategy for MMC-HVDC Systems With Hybrid DC Circuit Breakers. *IEEE Trans. Power Deliv.* **2020**, *35*, 1111–1123. [[CrossRef](#)]
180. Song, G.; Wang, T.; Hussain, K.S. DC Line Fault Identification Based on Pulse Injection From Hybrid HVDC Breaker. *IEEE Trans. Power Deliv.* **2019**, *34*, 271–280. [[CrossRef](#)]
181. Yang, S.; Wen, J.; Xiang, W. A Fault identification Method for MMC based DC Grids with Hybrid DCCBs. In Proceedings of the 2020 IEEE Power & Energy Society General Meeting (PESGM), Virtual, 2–6 August 2020. 2020.9281927. [[CrossRef](#)]
182. Zhang, S.; Zou, G.; Li, B.; Xu, B.; Li, J. Fault property identification method and application for MTDC grids with hybrid DC circuit breaker. *Int. J. Electr. Power Energy Syst.* **2019**, *110*, 136–143. [[CrossRef](#)]
183. Kontos, E.; Pinto, R.T.; Rodrigues, S.; Bauer, P. Impact of HVDC Transmission System Topology on Multiterminal DC Network Faults. *IEEE Trans. Power Deliv.* **2015**, *30*, 844–852. [[CrossRef](#)]
184. Leterme, W.; Pirooz Azad, S.; Van Hertem, D. HVDC grid protection algorithm design in phase and modal domains. *IET Renew. Power Gener.* **2018**, *12*, 1538–1546. [[CrossRef](#)]
185. Bucher, M.K.; Wiget, R.; Andersson, G.; Franck, C.M. Multiterminal HVDC Networks—What is the Preferred Topology? *IEEE Trans. Power Deliv.* **2014**, *29*, 406–413. [[CrossRef](#)]
186. Jahn, I.; Chaffey, G.; Svensson, N.; Norrga, S. A holistic method for optimal design of HVDC grid protection. *Electr. Power Syst. Res.* **2021**, *196*, 107234. [[CrossRef](#)]

187. Akhmatov, V.; Callavik, M.; Franck, C.M.; Rye, S.E.; Ahndorf, T.; Bucher, M.K.; Müller, H.; Schettler, F.; Wiget, R. Technical Guidelines and Prestandardization Work for First HVDC Grids. *IEEE Trans. Power Deliv.* **2014**, *29*, 327–335. [[CrossRef](#)]
188. Liu, Z.; Mirhosseini, S.S.; Popov, M.; Audichya, Y.; Colangelo, D.; Jamali, S.; Palensky, P.; Hu, W.; Chen, Z. Protection Testing for Multiterminal High-Voltage dc Grid: Procedures and Assessment. *IEEE Ind. Electron. Mag.* **2020**, *14*, 46–64. [[CrossRef](#)]
189. CIGRE Working Group B4.56. TB 657: Guidelines for the Preparation of “Connection Agreements” or “Grid Codes” for Multi-Terminal Schemes and DC Grids. 2016. Available online: <https://e-cigre.org/publication/657-guidelines-for-the-preparation-of-connection-agreements-or-grid-codes-for-multi-terminal-schemes-and-dc-grids> (accessed on 30 October 2022).
190. CIGRE Joint Working Group A3/B4.34. TB 683: Technical Requirements and Specifications of State-of-the-Art HVDC Switching Equipment. 2017. Available online: <https://e-cigre.org/publication/683-technical-requirements-and-specifications-of-state-of-the-art-hvdc-switching-equipment> (accessed on 30 October 2022).
191. CIGRE Working Group B4.57. TB 604: Guide for the Development of Models for HVDC Converters in a HVDC Grid. 2014. Available online: <https://e-cigre.org/publication/604-guide-for-the-development-of-models-for-hvdc-converters-in-a-hvdc-grid> (accessed on 30 October 2022).